Addressing Thermal Challenges in Rotary-Airlock Valves: An Industrial Perspective

Thesis Submitted in partial fulfillment of the Requirements for the degree of

Master of Engineering

in

Thermal Engineering

by

Altaf Raja Warshi

Registration No.: 802383001

Under the Supervision of

Dr. Anu Mittal
(Assistant Professor, MED)
Dr. Deepa Mudgal
(Associate Professor, MED)
Mr. Johnson Rego
(Industry Mentor, RIECO Industries Ltd)

MECHANICAL ENGINEERING DEPARTMENT

THAPAR INSTITUTE OF ENGINEERING & TECHNOLOGY, PATIALA

August 2025

Certificate

I **Altaf Raja Warshi** hereby certify that the work which is being presented in this thesis, entitled "Addressing Thermal Challenges in Rotary Airlock Valves: An Industrial Perspective" in fulfillment of the requirements for the award of the Degree of Master of Engineering in Thermal Engineering submitted to the Mechanical Engineering Department, Thapar Institute of Engineering and Technology, Patiala is an authentic record of my work under the supervision of Dr. Anu Mittal, Assistant Professor, Dr. Deepa Mudgal, Associate Professor at Mechanical Engineering Department, Thapar Institute of Engineering &Technology, Patiala and Mr. Johnson Rego, RIECO Industries Ltd.

The matter presented in this report has not been submitted anywhere for the award of any other degree by this or any other University/Institute.

Altaf Raja Warshi

Dated: 29/07/2025

Altaf Raja Warshi
(802383001)

It is certified that the student's above statement is correct to the best of my/our knowledge and belief.

29/7/25

Dr. Anu Mittal,
Assistant Prof. (M.E.D)
T.I.E.T, Patiala.

30/07/2025

Dr. Deepa Mudgal,
Associate Prof. (M.E.D)
T.I.E.T, Patiala.

Acknowledgement

I would like to specially acknowledge and extent my heartfelt gratitude to all those who have helped me in completion of this thesis. I would especially would like to thanks Dr. Anu Mittal, Assistant Professor, Dr. Deepa Mudgal, Associate Professor, Mechanical Engineering Department, Thapar Institute of Engineering and Technology, Patiala. Mr. Johnson Rego, General Manager, New Product Development, Rieco Industries Ltd., for their support and guidance. Furthermore, I am grateful to our team of New Product Development, Rieco Industries Ltd. For their support at every step. I would also like to thanks my parents for their love, support and encouragement in every step of my life. They have always wanted the best for me and I admire their determination and sacrifices. Besides, I would like to my institute i.e., Thapar Institute of Engineering and Technology. Rieco Industries Ltd. Pune is gratefully acknowledged for providing the best platform for research. Last but not least; I would like to thank the God for all their good benevolence.

List of Tables

List of Figures

Nomenclature:

Symbol	Description	Units
$\boldsymbol{A}$	Heat Transfer Area	m^2
$\boldsymbol{c}$	specific heat capacity of the rotor	(J kg^{-1} $°C^{-1}$)
$\boldsymbol{d}$	Diameter of particles	m
$\boldsymbol{h}$	Heat-transfer coefficient	W m^{-2} $°C^{-1}$
$\boldsymbol{L}$	Length	m
$\boldsymbol{T}$	Temperature	°C
$\boldsymbol{r}$	Coordinate axis	m
$\boldsymbol{\theta}$	Coordinate axis	Rad
$\boldsymbol{\rho}$	Density	Kg/m^3
$\boldsymbol{t}$	Time	sec
$\boldsymbol{k}$	Thermal Conductivity	W m^{-1} $°C^{-1}$
$\boldsymbol{\sigma_g}$	Molecules mean free path	m
$\boldsymbol{\Gamma}$	Particle Surface roughness	m
$\boldsymbol{\varphi}$	Wall area covered by particle	-
$\boldsymbol{\chi}$	Dimensionless gas film thickness	-
$\boldsymbol{\alpha}$	Thermal Diffusivity	m^2/s
$\boldsymbol{\theta_{pocket}}$	Angle subtended by one pocket	Rad
$\boldsymbol{N}$	Angular Speed	RPM

Superscripts

Pl	:	Penetration Layer
C	:	Conduction

Subscripts

R or r	Rotor
p	Powder particles
a	Air
c	Conduction
g-w	Gas-wall conduction
p-w	Particle-to-wall conduction
b-w	Bulk bed-to-wall total contact conductance

Table of Contents

Contents

ABSTRACT

Rotary airlocks are pivotal components in a wide range of industrial systems, serving the dual function of regulating material flow and maintaining pressure differentials between connected environments. Due to their ability to prevent air leakage while enabling consistent material transfer, which is critical to the reliable pneumatic conveying of bulk materials in various sectors such as food processing, chemical manufacturing, cement production, and pharmaceuticals. At the heart of a rotary airlock is a cylindrical rotor fitted with multiple vanes that create sealed compartments, enabling the controlled transfer of materials from the inlet to the outlet while maintaining pressure isolation. In industrial applications—particularly those involving a wide range of powders and varying operating temperatures—rotary airlocks face several performance challenges. These include air leakage, thermal expansion, material jamming, and accelerated wear, especially when dealing with abrasive or cohesive materials. Such challenges can compromise efficiency, reliability, and the overall lifespan of the equipment, making robust design and regular maintenance essential. In high-temperature environments, such as cement kilns or chemical reactors, thermal effects further complicate performance by altering component clearances and weakening sealing integrity, which in turn can degrade system functionality and increase the risk of failure. Recent research underscores the critical importance of understanding heat transfer and thermal behavior in rotary systems, emphasizing the need for accurate thermal modeling to minimize efficiency losses and prevent operational failures. In this context, the present study investigates the thermal characteristics of rotary airlocks, with a particular focus on analyzing heat transfer mechanisms, thermal expansion effects, and their influence on air leakage and rotor-to-casing clearance. By incorporating insights from recent advancements, this work aims to contribute to the development of improved design strategies and to enhance the reliability and performance of rotary airlocks operating in thermally challenging industrial environments.

Keywords: rotary air-lock, air leakage, rotor-to-housing clearance, thermal expansion, thermal behavior

CHAPTER 1: INTRODUCTION

1.1 Introduction

Rotary airlocks are the mechanical devices used to control the bulk material transfer between two chambers operating at different pressures, while minimizing the air leakage[1]. These devices are crucial components of pneumatic conveying systems in various industries such as food processing, chemical manufacturing, cement production, and pharmaceuticals, where accurate material flow control and pressure isolation are critical for operational efficiency. The primary function of a rotary airlock is to control the flow of materials while keeping the pressure difference between connected systems [2]. It allows continuous movement of material without air leakage and keeps the system working properly. They feed materials into reactors, remove solids from hoppers or silos, and keep pressure levels separate in air-based systems [3]. In cement plants, they handle hot, rough materials. In chemical and pharmaceutical industries, they provide accurate and airtight feeding. In food processing, they help with the clean and steady flow of ingredients like flour or sugar. Power plants use them to feed coal or ash, and they are also used in dust collectors to remove trapped particles.

The rotary airlock is made up of a cylindrical rotor with several vanes or blades that form sealed compartments, also known as pockets, for material handling. As the rotor rotates within its housing, the pockets move materials from the intake to the outlet while keeping a pressure differential. This pressure-sealing feature is critical in pneumatic conveying systems, which use pressurized air to deliver materials such as powders, flour, and cement, as well as coarse granules like pellets and fertilizers. A rotary airlock must be precisely designed, as its performance directly affects the overall efficiency of the system. Minimizing air leakage and maintaining a steady flow of material helps reduce energy losses and ensures reliable, uninterrupted operation [4].While designing rotary airlocks, it is essential to consider several critical parameters that influence their efficiency and durability. Despite their sturdy construction and widespread use, rotary airlocks can face performance and reliability issues [5]

such as air leakage, thermal expansion, material jamming, and wear caused by abrasive or cohesive materials. Addressing these factors during the design stage is vital to ensure minimal energy loss, consistent material flow, and long-term operational stability in demanding industrial

environments. Air leakage in rotary airlocks disrupts pressure balance in pneumatic systems, reducing conveying efficiency and increasing energy consumption. High-temperature applications, such as in cement kilns or chemical reactors, pose additional challenges as thermal expansion can alter clearances and sealing effectiveness [6]. Uneven expansion between components may lead to increased wear, reduced sealing, and overall operational inefficiencies. Although there could be several measures to avoid these issues, for example, material jamming could be addressed by blade beveling, flexible seals, and venting moist air, etc.[7] Further, excessive air leakage could be controlled by optimizing the rotor and housing clearance. For that purpose, it becomes important to know the air leakage through the rotary air lock operating corresponding to varied amounts of differential pressures. In a study by Roger et al. [8], an analytical model was developed to predict air leakage rates, and it was found that the leakage rate is directly proportional to the pressure differential across the airlock. Many researchers have suggested ways to reduce air leakage, such as reduced clearance and adjustable blade tips [1][9]. There could also be other issues, including backflow of low-density particles into the hopper due to pressure imbalances, sticking of particles within the rotor pockets as a result of frictional heating, and flow blockages caused by the formation of cohesive arches of granular material. A modified design was suggested with the provision of a flexible pressure balancing tube between the top of the particle storage hopper and the airflow line just upstream of the feeder, and a circular slot eccentric to the valve housing [10]. In an effort to minimize air leakage through rotary airlocks, designers often aim to reduce the rotor-to-housing clearance; however, this approach can have adverse effects in high-temperature applications. As the temperature rises, both the rotor and housing components undergo thermal expansion, which can significantly reduce the already narrow clearance. This may lead to mechanical interference, increased friction, and even seizure of the rotor, ultimately compromising the reliability and efficiency of the airlock. Therefore, while tighter clearances help reduce leakage, they must be carefully balanced with allowances for thermal expansion to ensure safe and stable operation under elevated temperatures. Handling combustible dust may further aggravate the issues related to the operational safety of rotary air locks. The size and shape of the gap between the rotor and the housing play a critical role in either allowing or preventing an explosion from spreading [11].Therefore, it is important to carry out thermal analysis for rotary airlocks in order to assess temperature-induced deformations and clearance variations, thus enabling design improvements for enhanced durability, reliability, and performance under high-

temperature operating conditions. In such applications, it becomes important to understand the major heat transfer mechanisms during rotary airlock operation. The insights from a study by Wang et al. [12] on heat transfer in a rotary ash cooler can also be valuable for understanding and improving the thermal performance of rotary airlocks in high-temperature applications like ash handling systems. Similar to rotary coolers, rotary airlocks in such systems are exposed to hot particulate matter and are subject to complex heat transfer phenomena. The finding [12] that ash-to-wall conduction and radiation dominate heat transfer suggests that in rotary airlocks, the rotor and housing surfaces are also key pathways for heat exchange, which can influence material selection and cooling strategies. Additionally, the observation that smaller particle sizes and higher rotation speeds enhance heat transfer by reducing thermal resistance can be extrapolated to rotary airlocks, indicating that finer particles and optimized rotational speeds might lead to more uniform temperature distribution, reducing hot spots that cause thermal expansion issues. These inputs help in designing thermally stable rotary airlocks by allowing better prediction of heat loads and guiding the incorporation of thermal compensation features to maintain clearances and avoid performance degradation. Another study by Zhang et al. [13] on packed bed-to-wall heat transfer offers useful insights for rotary airlocks handling hot granular materials. Despite differences in system design, geometry, and flow conditions, both systems involve heat exchange between solid particles and surrounding walls, making the underlying mechanisms, such as particle-to-wall conduction and the influence of particle size and temperature, applicable. In rotary airlocks handling hot solids, heat transfer from the bulk material to the rotor and housing plays a key role in determining temperature rise, thermal expansion, and potential sealing issues. Key findings [13]—such as enhanced heat transfer with smaller particles and higher temperatures—can help predict thermal loads and guide the design of airlocks, particularly in managing thermal expansion, material selection, and clearance tolerances for high-temperature operations.

Nagulmeera and Anilkumar [14] conducted a study on the design and structural analysis of a rotary airlock to ensure its reliable performance under demanding conditions like high pressure and high temperature. They created a 3D model of the valve using Pro-E (Creo) software and performed finite element analysis (FEA) using ANSYS to evaluate how the shaft behaves under operational loads. Their analysis focused on key mechanical parameters such as shaft deflection and stress distribution. The simulation results showed a maximum shaft deflection of 0.041 mm, which was within acceptable safety limits, indicating that the structure would not deform

excessively during operation. Based on this, they calculated a factor of safety (FoS) of 1.45, confirming that the design is mechanically sound and capable of withstanding expected stresses without failure. Based on the current literature, it is evident that most studies on rotary airlocks primarily focus on air leakage estimation through empirical modeling and experimental testing. However, research addressing the thermal behavior of rotary airlocks remains limited. Therefore, the present study aims to bridge this gap by conducting analytical modeling and simulation to investigate the thermal characteristics and heat transfer mechanisms within a rotary airlock, particularly under high-temperature operating conditions.

Figure 1.1 Rotary Airlock

Figure 1.2 Removable Rotor

1.2 Key Features and Functions

Rotary airlocks are designed with certain features to meet industrial requirements. One important role is pressure isolation, which ensures a consistent pressure differential between two chambers, maintaining the process's integrity. This feature is significantly important in pneumatic conveying

systems, where pressure stability is essential for material movement. Furthermore, rotary airlocks are versatile in handling a wide range of materials, including fine powders such as flour and cement, as well as coarse granules like pellets and fertilizers. They can be customized to manage abrasive, corrosive, or high-temperature materials. High-temperature rotary airlocks, for example, can withstand operating conditions of up to 300°C or higher, depending on their design and materials. Additionally, rotary airlocks enhance energy efficiency and system reliability by reducing air and material leakage, even under extreme operating conditions.

1.3 Importance of Rotary Airlocks

Rotary airlocks have an important role in modern industries where precise material handling is critical. For instance, they are indispensable in feeding material into reactors, discharging from hoppers, or isolating distinct pressure zones in pneumatic systems. Rotary airlocks prevent material clogging and ensure smooth operation in industries such as cement and chemicals. These devices address several challenges, including preventing material contamination during transfer, allowing controlled material discharge, and adapting to conditions such as high temperatures or abrasive material handling. By maintaining pressure isolation and regulating flow, rotary airlocks reduce energy consumption and enhance equipment longevity, thereby contributing to continuous and efficient operations.

1.4 Classification of Rotary Airlocks

Rotary airlocks are classified based on their design and application, each suited to specific industrial needs. Below is a detailed description of the main types of rotary airlocks:

Drop-Through Rotary Airlocks

Drop-through rotary airlocks are designed for free-flowing materials. In these systems, materials discharge through the valve under gravity or with the assistance of air pressure. These rotary airlocks are mostly employed in pneumatic conveying systems for handling powders or granules. Their simple design makes them the perfect choice for applications that need great reliability with lower maintenance. Industries such as cement production and grain processing often prefer drop-through airlocks due to their effectiveness and ease of use.

Blow-Through Rotary Airlocks

Blow-through rotary airlocks require a stream of air to force materials through the valve. This type of rotary airlock works very effectively in pneumatic conveying systems where material flow needs to be continuous and uninterrupted. The air stream ensures that the material does not accumulate in the valve, thus preventing clogging and maintaining efficient operation. Blow-through rotary airlocks are widely used in industries dealing with fine powders, such as flour, sugar, or chemicals. The integration of air streams also reduces the risk of material bridging, ensuring a smooth and consistent transfer process.

Offset Rotary Airlocks

The design of offset rotary airlocks is such that the rotor is positioned off-center relative to the housing. This design minimizes direct airflow across the valve, effectively minimizing the air leakage and cross-contamination between the inlet and outlet chambers. Offset airlocks are frequently useful in systems requiring tight seals and minimal leakage, such as those handling hazardous or fine powders. Their unique design makes them suitable for industries like pharmaceuticals, where contamination control is critical.

Custom Rotary Airlocks

Custom rotary airlocks are designed to meet certain specific industrial requirements. For example, high-temperature rotary airlocks are designed with insulated housing and rotors that can resist elevated temperatures exceeding 500°C. Food-grade rotary airlocks, in contrast, use polished stainless steel and FDA-approved seals to meet hygiene standards. Customization of designs is made to handle abrasive or corrosive materials, increasing the equipment's operational life. While these solutions are typically more expensive, they provide enhanced performance and reliability for challenging environments.

1.4 Significance in Thermal Analysis

High-temperature operations imposes critical engineering challenges for rotary airlocks, particularly in industries such as cement manufacturing, chemical processing, and power generation. These devices are subjected to extreme thermal environments where the uneven heating of components can severely affect their operational integrity. Rotary airlocks, responsible for controlling the flow of bulk materials while isolating differing pressure zones, must maintain tight clearances to function effectively. However, under elevated temperatures, thermal expansion of materials can compromise these critical tolerances, leading to diminished performance and, in some cases, mechanical failure.

Thermal analysis plays an important role in understanding and mitigating the adverse effects of high-temperature exposure on rotary airlocks. This analytical approach involves the study of temperature distribution across the rotary airlock components and how these thermal gradients influence material behavior. For example, the rotor, typically made from a metal alloy, may expand differently compared to the housing or end plates, resulting in misalignment or seizure. Without proper design accommodations, these thermal mismatches can cause increased friction, accelerated wear, leakage, or complete breakdown of the airlock.

One of the primary concerns in high-temperature applications is the reduction of rotor-to-housing clearances. These clearances are essential for the unimpeded rotation of the rotor and for maintaining a pressure seal between different compartments. As components expand due to heat, the gap narrows, sometimes to the point of contact. This not only results in mechanical wear but also leads to increased energy consumption as the system compensates for the additional resistance. Moreover, material degradation due to excessive heat can further exacerbate these issues, especially if the materials are not adequately rated for the operational temperature range.

To address these issues, engineers employ finite element analysis (FEA) and computational fluid dynamics (CFD) as part of the thermal analysis process. These simulation tools allow for a detailed examination of heat transfer mechanisms within the airlock, including conduction, convection, and radiation. By modeling the temperature profiles under various operating conditions, designers can predict deformation patterns and stress concentrations. This data is crucial for optimizing component geometries, selecting appropriate materials, and incorporating thermal expansion joints or insulation where necessary.

Material selection is another critical outcome of thorough thermal analysis. The ideal materials for rotary airlocks in high-temperature environments must possess not only high thermal resistance but also favorable mechanical properties such as strength, hardness, and resistance to thermal fatigue. Commonly used materials include high-grade stainless steels, nickel-based alloys, and ceramics. Each of these materials reacts differently to heat, and their selection is often guided by the results of thermal modeling. Additionally, coatings or surface treatments may be applied to enhance the thermal resistance or reduce the coefficient of friction under elevated temperatures.

In some designs, active or passive cooling systems are incorporated to regulate the temperature of sensitive components. Thermal analysis helps in the design and placement of these systems to ensure optimal performance. For instance, air or liquid cooling channels may be embedded within the housing, or heat shields may be strategically placed to deflect radiant heat away from critical parts.

These interventions, informed by precise thermal data, significantly improve the lifespan and reliability of rotary airlocks.

Another important aspect of thermal analysis is the understanding of thermal cycling and its long-term effects. Industrial processes often involve heating and cooling cycles that cause materials to expand and contract repeatedly. This can lead to thermal fatigue, micro-cracking, and eventual failure if not properly accounted for during design. By simulating these cycles, engineers can estimate the service life of rotary airlocks and schedule maintenance or replacements before failures occur.

Furthermore, thermal analysis aids in developing compensatory design strategies such as the use of tapered clearances, floating end plates, and flexible seals that can adapt to dimensional changes. These features allow the airlock to accommodate thermal expansion without compromising functionality. Some advanced designs even incorporate smart sensors that monitor temperature in real-time and adjust operating parameters accordingly, such as slowing rotor speed or increasing ventilation to avoid overheating.

In essence, the integration of thermal analysis into the design and evaluation of rotary airlocks ensures that these components can withstand the rigors of high-temperature industrial environments. It leads to the development of robust, reliable systems that not only maintain performance under stress but also reduce downtime, maintenance costs, and energy consumption. This is particularly important in industries where process continuity and efficiency are paramount.

In conclusion, rotary airlocks are indispensable components in modern industrial systems, ensuring the controlled transfer of materials while maintaining pressure differentials and system integrity. Their performance directly influences the efficiency and reliability of critical processes, particularly under extreme temperature conditions. Thermal analysis emerges as a key tool in overcoming the engineering challenges associated with high-temperature operations. By enabling precise prediction and mitigation of thermal effects, it supports the development of innovative airlock designs that are durable, efficient, and adaptable to demanding applications. As industries continue to push operational boundaries, ongoing research and innovation in thermal analysis and material science will remain central to advancing the design and functionality of rotary airlocks.

CHAPTER 2: LITERATURE REVIEW

2.1 Literature Review

Richard Siwek (1989) investigated the ignition of combustible dust within the clearance of the airlock and proposed a modification in design to mitigate the hazard. The study identifies the critical parameters, such as gap width, gap length, and rotor vane design, that are essential in preventing explosions. The major contribution was the introduction of the concept of maximum experimental safe gap (MSEP) that is permissible to prevent an explosion. The explosion was simulated experimentally with dust particles having distinct ignition properties. The result demonstrated that smaller gap size and higher vane coverage enhance the ability of rotary airlocks to prevent ignition breakthrough effectively [15]

Ray Galuska (1997) explored key operational challenges in rotary airlock valves and proposed actionable strategies to enhance their performance. He identified four primary issues—jamming, excessive air leakage, noisy operation, and insufficient material throughput—and provided targeted solutions for each. To address jamming, which may result from rotor rotation issues, thermal expansion, or material interference, the suggested remedies include blade beveling, flexible seals, and venting moist air. Excessive air leakage was mitigated by reducing clearances between the rotor and casing. For noisy operation, often caused by material buildup, rotor expansion, or improper storage, solutions such as interior coating, frequent polishing, and blade tip beveling were recommended [7]

Roger et al. (2000) developed an analytical model to predict air leakage rates through rotary airlocks operating under differential pressure. The model is founded on the principle of airflow through multiple orifices in series, where the clearances between rotor blades and the casing are treated as sequential orifice plates. Using Bernoulli's equation, the model estimates leakage rates for various rotor configurations, including open-end, sealed, closed-end, and unsealed closed-end designs. Validation against experimental data demonstrated deviations within 6–10% across these configurations, underscoring the model's reliability. The findings highlight that the leakage rate is directly proportional to the pressure differential across the airlock. Additionally, minimizing the clearance between the rotor blades and the casing significantly reduces the leakage rate, as the clearance acts as a primary factor influencing airflow. Furthermore, increasing the number of blades

effectively reduces leakage by introducing more flow restrictions. These insights make the model particularly useful for optimizing rotary airlock designs for pneumatic conveying systems [8]

Gundogdu et al. (2004) address the critical issues in conventional rotary airlocks employed for feeding material, especially granular material, by modifying the design of the airlock to enhance its performance. The major issues are—the backflow of low-density particles into the hopper due to pressure imbalances, the sticking of particles within the pocket caused by frictional heating, and flow obstructions due to the formation of cohesive particle arches.

The backflow of particles and flow obstruction can be handled by incorporating a flexible pressure tube between the top of the hopper and the upstream airflow line of the feeder. The particle stickiness issue is also solved by carving an eccentric slot into the housing of the airlock to enhance air circulation and reduce overheating. Increasing the number of vanes in the rotary feeder helps in solving the low feeding rate of material. The experimental studies demonstrate that the modified airlock effectively handles material feeding in the range of 5 ± 0.15 to 85 ± 0.85 g/s without any operational disruption. There is also an improvement in the reproducibility of adjustable particle mass feeding rates from ±3% to ±1%, with the increase in rotational speed [10]

Jonathan et al. (2007) investigated the pressing issues in pneumatic conveying systems (i.e., air focusing on air leakage through rotary airlocks. The objective is to mitigate the challenges caused by leakage air, such as reduced material flow, dust release, and pressurization of upstream equipment, which significantly disrupt the operation. The study provided six practical ways to tackle air leakage through the airlock, tailoring each method to specific material properties and operating conditions. For instance, the Direct Connection to Storage Vessel method is designed for porous materials and fluidized powders at low pressures, where leakage air is vented directly into the storage vessel, allowing it to pass through the stored material and exhaust via a bin vent filter. Another method, the Vent Surge Hopper, involves attaching an additional surge hopper with a vent filter to the top of the airlock. This configuration facilitates the removal of leakage air through the vent filter and is particularly handling pellets and granules in systems operating at pressures above 8 psig [16]

Wypych et al. (2008) comprehensively studied the air leakage of rotary airlocks and their impacts on pneumatic conveying systems, developing a new theoretical model for both conventional and high-

pressure valves. The model highlights the influences of critical parameters such as pressure, rotor clearances, material properties, and venting configuration. Air leakage impacts the feeding of material, particularly in the case of dense phase conveying.

To alleviate leakage, different techniques such as minimizing rotor-to-housing clearance and utilizing adjustable blade tips are proposed. The predicted value of air leakage with this model shows a remarkable accuracy of ±6% compared to experimental data, which contrasts with older models and supplier curves having errors in the range of -48% and +39%. Additionally, the research also demonstrates the reduction in air leakage and increase in feeding capacity by incorporating vent hoppers [4]

Wang et al. (2010) have formulated a one-dimensional mathematical model to study the heat transfer in a rotary ash cooler used in circulating fluidized boilers. The study evaluates the major heat transfer modes within rotary ash coolers—conduction, radiation between hot ash and roller wall, and convection due to leaked air. The analysis reveals that ash-to-wall heat transfer is the dominant mechanism, accounting for over 80% of total heat transfer. Furthermore, the smaller particle sizes and faster rotational speeds were found to reduce thermal resistance and thus enhance heat transfer. The model was validated experimentally and has been found that the predicted value of heat transfer coefficient and outlet temperature align closely with industrial data, with a discrepancy within ±10%, ensuring the model's reliability [12]

Somsuk et al. (2012) designed and developed a rotary airlock valve with minimum clearance between rotor tips and housing, along with adjustable and replaceable rotor blades mounted on rotor shafts with a packing seal to minimize air leakage during continuous feeding of material in a continuous pyrolysis process. Their study indicates that the pressure differential varies with rotational speed, and the new design approximately achieved a 60% improvement in air locking efficiency as compared to the conventional one. The improvement is crucial in the pyrolysis process as it correlates with efficient material feeding and better product yields [1]

Zhang et al. (2013) developed a predictive heat transfer model to investigate the mechanisms governing heat transfer between a packed bed and an adjacent wall in heat recovery processes. The study aimed to enhance the design and operational efficiency of packed bed reactors, which are widely

utilized for cooling, heating, and drying operations across various industries.

Their work introduced a one-dimensional bed-to-wall heat transfer model that integrates particle-to-wall heat conduction and conduction through the thermal penetration layer. A sensitivity analysis was conducted to evaluate the effects of key parameters on the heat transfer coefficient. It was observed that the heat transfer coefficient increases with temperature due to enhanced radiation effects and higher material conductivity at elevated temperatures. Additionally, smaller particle sizes were found to improve heat transfer efficiency by increasing the surface area available for conduction.

The model was validated against experimental results, demonstrating that 95% of the predicted data fell within a ±20% accuracy range, affirming the reliability of the proposed model [13]

Nagulmeera et al. (2013) studied comprehensively the design, modelling, and analysis of the rotary airlock. Their work focuses on the optimization of design to ensure reliability under challenging conditions such as high pressure and high temperature. The author modelled the rotary airlock valve using Pro-E software and did the finite element analysis using Ansys to determine the shaft deflection and stress distribution. The result showed a deflection of 0.041mm, which is under the safe limit, and based on this value factor of safety is determined to be 1.45, which ensures the robustness of the valve [14]

2.2 Gaps in Literature

Despite extensive research into the mechanical, operational, and safety aspects of rotary airlocks, a significant gap remains in the comprehensive thermal analysis of these devices, especially when operating under high-temperature and high-pressure industrial conditions. The reviewed literature highlights valuable contributions to explosion mitigation, leakage reduction, performance optimization, and component redesign. However, it collectively lacks a systematic and integrated thermal framework that combines heat transport, thermal expansion, and pressure dynamics specific to rotary airlocks.

Most of the existing studies approach the topic from isolated angles. For example, Siwek [15] primarily focused on explosion safety by analyzing gap width and ignition behavior but did not account for the effects of temperature-induced deformation on gap integrity. Galuska [7] and Gundogdu [10] addressed mechanical problems such as jamming and material backflow, offering

practical modifications like flexible seals or venting solutions. Yet, these studies overlooked how sustained high temperatures influence material wear, thermal fatigue, and the behavior of these modified designs over time.

Air leakage, a common concern in rotary airlock performance, has been modeled analytically by Roger [8] and Wypych [4] who offered predictive models based on geometry and pressure differentials. However, their analyses remain largely isentropic and isothermal**,** lacking consideration of how thermal expansion alters the critical rotor-to-housing clearances that govern leakage. In real-world industrial scenarios—such as in pyrolysis, ash handling, or cement manufacturing—airlocks operate under fluctuating thermal loads. This thermal stress not only affects clearances but also influences material strength, sealing performance, and airflow turbulence, which existing models do not capture.

Some progress has been made in incorporating heat transfer analysis into rotary systems, such as in the works of Wang [12] and Zhang [13]. These studies modeled heat transfer through conduction, convection, and radiation in specific equipment like rotary ash coolers and packed beds. However, the models were limited to one-dimensional assumptions or static geometries and did not fully account for the rotational behavior, dynamic contact surfaces, and real-time thermal deformation of a rotary airlock under working conditions.

Moreover, mechanical design optimization studies, such as those by Nagulmeera [14] employed finite element analysis (FEA) to assess stress and deflection in rotary components. While these models confirmed the structural integrity under pressure loads, they did not include thermal-mechanical coupling—a critical omission, as heat can significantly influence material behavior, alter stress distribution, and lead to expansion-induced failure mechanisms such as rotor seizing or excessive seal wear.

Therefore, it becomes evident that the combined effects of heat transfer, thermal expansion, and pressure variation on rotary airlocks remain underexplored. Specifically, no study to date has presented a unified model or experimental framework that simulates or predicts how high thermal loads interact with the airlock’s internal pressure, material flow dynamics, and component clearances. This is a critical omission, especially given the operational environments of many rotary airlocks, which frequently involve temperatures exceeding 300°C, rapidly cycling pressures, and abrasive or adhesive bulk materials.

Additionally, material behavior under thermal cycling and the long-term implications of such cycling on fatigue, warping, and sealing efficiency are not sufficiently addressed. Industrial airlocks often experience rapid startup and shutdown sequences, causing fluctuating thermal gradients that can degrade both metallic and polymer components over time. Without data-driven insights into these effects, current design practices rely heavily on conservative safety factors, which may lead to inefficient, overbuilt systems or premature failures.

To address these shortcomings, the development of an integrated thermal-structural-fluid framework is essential. This would include:

- Detailed heat transfer modeling (including conduction through solid parts, convective losses, and internal radiation),
- Simulation of thermal expansion and its effect on clearances and contact interfaces,
- Coupled analysis of internal pressure changes and material flow behavior under elevated temperatures,
- Consideration of transient (non-steady-state) thermal and pressure conditions to mimic real industrial processes,
- Experimental validation of model predictions with temperature, pressure, and deformation measurements.

By filling these gaps, researchers and engineers can design rotary airlocks that are not only mechanically robust but also thermally optimized for high-efficiency operation in extreme environments. A reliable thermal analysis framework would enable improved material selection, more accurate lifespan prediction, reduced maintenance requirements, and higher energy efficiency. It would also pave the way for the development of smart airlock systems capable of adjusting operational parameters in real time based on thermal conditions.

In conclusion, while the literature provides a foundational understanding of airlock operation, the lack of a comprehensive thermal analysis model that integrates with pressure and flow dynamics represents a major limitation. The proposed research aims to bridge this gap by developing and validating such a model, thereby enhancing the operational efficiency, safety, and reliability of rotary airlocks in high-

temperature and high-pressure industrial applications.

2.3 Objectives of the Work

The focus of the thesis is to investigate and address the thermal challenges associated with rotary airlocks operating under elevated temperature industrial conditions. To achieve this, the core objectives of the work are as follows:

- ✓ Analyze thermal challenges in rotary airlocks at high temperatures.
- ✓ Develop a mathematical model for heat transfer.
- ✓ Investigate influence of blade and material parameters.
- ✓ Model powder-air interactions for localized heating.

Through this thesis we aim to address the thermal challenges faced by rotary airlocks in high-temperature industrial applications. One of the key aspects is to quantify the distribution of heat across the rotor, as this affects both performance and longevity. A comprehensive mathematical model will be developed to simulate heat transfer under both transient and steady-state conditions, providing insights into thermal behavior and assisting in the design optimization of airlocks. As thermal expansion is a critical concern, the impact on rotor-to-housing clearances will be evaluated to ensure proper functioning during thermal cycles. Additionally, the influence of critical design parameters such as blade thickness, blade angle, and material properties on thermal performance will be explored. The study will also examine the temperature effects on the major components, specifically the rotor and housing, to assess their resilience under high thermal stress. To accurately solve the heat conduction equations, finite difference methods (FDM) will be applied within the geometry of the rotary airlock. Furthermore, the interaction between the powder and air phases will be modeled to predict localized heating, providing a more detailed understanding of the thermal profiles and their impact on overall performance.

CHAPTER 3: NUMERICAL ANALYSIS

3.1 Mathematical Model

The mathematical model for heat transfer in rotary airlock valves is developed to predict how temperature changes over time within the rotating blades and housing as they move between hot powders and cooler air. The model uses the heat diffusion equation to predict transient heat conduction behavior and to describe how heat spreads through the metal, considering the specific properties of materials like mild steel and SS316 stainless steel, which heat up and cool down at different rates. As the temperature of housing and rotor rises and falls, they expand and contract, which can change the gap between the rotor and housing-potentially leading to air leaks or mechanical interference. By simulating these processes, the model helps engineers design rotary airlock valves that maintain proper sealing and reliable operation even under demanding thermal conditions.

The following assumptions have been made while developing the heat transfer model:

a. The temperature of powder and air is uniform throughout the operation.

b. The air and powder have consistent properties (e.g., density, thermal conductivity) throughout.

c. Powder in rotor pockets behaves like a static, tightly packed solid (no particle movement).

d. The material of the rotor and casing is homogeneous.

e. The rotor interacts with either powder (loading side) or air (return side), not both at once.

f. The blade and shaft are at the same temperature where they meet, and the blade's base is insulated.

g. The system eventually stabilizes at a steady temperature after a certain time duration.

h. Radiation heat transfer is neglected.

The thermal energy balance for the rotary airlock system is expressed as:

$$\text{Change in energy of rotor} = \text{Rate of energy input from powder} - \text{Rate of energy lost to air}$$

The heat conduction equation in cylindrical coordinate system is given as follows:

$$\rho_R c_R \frac{\partial T}{\partial t} = \frac{h_{overall,p}}{L}(T_p - T_R) + k_R\left(\frac{1}{r}\frac{\partial}{\partial r}\left(r\frac{\partial T(r,\theta,t)}{\partial r}\right) + \frac{1}{r^2}\frac{\partial^2 T(r,\theta,t)}{\partial \theta^2}\right) - \frac{h_a}{L}(T_R - T_a) \quad (3.1)$$

Where the term on the left-hand side is representing the change in energy content of the rotor as a result of energy interaction between rotor, powder, and air by means of conduction and convection. The terms on the right-hand side is depicting those energy interactions by conduction and convection.

3.2 Simulation Setup

The rotor used in the study has an outer radius of 190 mm, an inner radius of 30 mm, and a length of 330 mm. Operating conditions include a powder temperature of 300°C, an air temperature of 80°C with a velocity of 9 m/s, and a rotor speed of 20 RPM. These parameters simulate realistic industrial conditions to ensure the applicability of the results. By combining theoretical modelling, and computational simulations, the methodology ensures a comprehensive understanding of thermal challenges in rotary airlocks and provides a robust foundation for design improvements.

Parameters: The temperature distribution of the rotary airlock is governed by several factors that affect the thermal behavior of the rotary airlock valve system. These parameters include geometrical measurements, heat transfer characteristics, and material properties.

Geometrical Dimensions: Rotary Airlock was modeled with defined geometrical measurements, which include the following...

Inner Radius (r_inner) = 0.030 meters, representing the radius of the shaft.

Outer Radius (r_outer) = 0.190 meters, representing the outer extent of the rotor.

Axial Length = 0.330 meters, length along the axial direction.

Blade Thickness = 0.008 meters, thickness of blade along the circumferential direction.

The angle between Blades = 36 degree / 0.628319 radian, the angle subtended by one pocket and obtained by dividing the angle covered in one complete rotation by the number of blades.

Number of Blades = 10,

Angular Speed = 20 rpm

These are the dimensions of PN 350 series RAL manufactured at Rieco Industries ltd.

Heat Transfer Parameters

Major parameters for heat transfer for both the powder and air phases were set up. Particle size, specific heat, bulk density, and thermal conductivities for the powder and air were determined. The heat transfer coefficients for the powder phases were calculated using the dimensionless gas film thickness and rotor angular speed.

Powder Phase: The heat transfer coefficient was derived using an effective approach considering contact conductance and overall heat transfer principles. It comprises of two parts—

a. Particle-to-particle heat transfer within the penetration layer is given as [12],[13]

$$h_{c\,(pl)} = 2 * \sqrt{\frac{k_p \rho_p C_p}{\pi t_c}} \tag{3.2}$$

Where, subscript 'p' refers to particle properties (which includes thermal conductivity, bulk density, and specific heat of particle) and 't_c' represents the contact time during which particle is in contact with rotor in a pocket and is determined by knowing the angle between two vanes and the rotational speed of the rotor and 'pl' stand for penetration layer.

b. Contact conductance: it includes the following:

Thermal conduction within the gas layer and conduction between particle and wall.

i. Conduction within gas film [13]

$$\mathrm{h}_{\mathrm{g-w}}^{\mathrm{c}} = \mathrm{k_g} / \left(\frac{\sqrt{2}\mathrm{d_p}}{2} + \sigma_{\mathrm{g}} \right) \tag{3.3}$$

Here, subscript 'g' stands for gas, in this case air, and 'w' for wall. σ_g refer mean free path of gas molecule.

ii. Particle-to-wall conduction [13]

$$h_{p-w}^{c} = \frac{4k_g}{d_p} \left\{ \left[1 + \frac{2(\sigma_g + \Gamma)}{d_p} \right] \ln \left[1 + \frac{d_p}{2(\sigma_g + \Gamma)} \right] - 1 \right\} \tag{3.4}$$

where, 'Γ' stands for particle surface roughness.

Total Contact conductance [13]

$$h_{b-w}^{c} = \emptyset_A h_{p-w}^{c} + (1 - \emptyset_A) h_{g-w}^{c} + h_{rad} \quad (3.5)$$

where, '$\emptyset_A$' stands for void space present within powder volume.

For packed bed plug flow, schlunder proposed another simplified formula for contact resistance, which is given by [12]

$$h_{b-w}^{c} = \frac{1}{\chi} \frac{k_g}{d_p} = \frac{1}{0.085} \frac{k_g}{d_p} \quad (3.6)$$

The overall particle-to-surface heat transfer coefficient is given as [12]

$$\boldsymbol{h_{overall,p}} = \left(\frac{1}{\frac{1}{h_{b-w}^{c}} + \frac{1}{h_c^{pl}}} \right) \quad (3.7)$$

Air Phase: A convective heat transfer coefficient of 15 was employed to characterize heat exchange with the air.

3.3 Discretization

Discretization means breaking the whole domain into finite-size elements. The objective of discretization is to make computation easier and more manageable. There are two ways to do discretization.

Finite Element Method (FEM): Where the whole domain is divided into small elements to make calculation easy

Grid Method: In this method domain is divided into discrete grid domains and problem is defined on a set grid point and the numerical method is used to solve the problem.

In this study, a grid discretization scheme was used, dividing the domain into radial, circumferential, and time components:

- *Grid Points (nr, ntheta):* Every pocket is divided into 90 radial and 10 circumferential grid points for spatial discretization.
- *Time Steps (nt):* The time taken by a pocket to complete a cycle is divided into 200 discrete time steps.

3.4 Assumptions

To simplify the analysis and focus on key thermal interactions, the following assumptions were made:

Steady-State and Transient Analysis:

We have assumed that the system attains a quasi-equilibrium state during its operation with high-temperature powder when the average temperature variation of the material of pockets

reaches the minimum defined value which in our case is 1E-2.

Homogeneous Material Properties:

It is assumed that the thermal properties (thermal conductivity, specific heat, etc.,) and physical properties of materials are constant and uniform throughout the analysis within each phase.

Two-Dimensional Heat Transfer:

In this model two-dimensional heat transfer is solved in the radial and circumferential direction, considering the temperature gradient in the axial direction as a minimum during each time step and within each pocket.

Perfect Mixing:

In this model, we have assumed that mixing is perfect in all directions within the pockets thus allowing us to consider the temperature of powder is uniform within the pockets and at any given time

Packed bed flow of powder within the pockets:

The flow of powder within the pockets is assumed to be a packed bed as the powder particles are not suspended within the pockets.

3.5 Boundary Conditions

Well-defined boundary conditions were assessed in accordance with heat transfer conditions at interfaces between the powder and the air, along with the rotor surface. The most critical thing in modeling thermal interaction within rotary airlock accurately is boundary conditions. In our case the following boundary conditions were applied:

Initial Conditions:

The temperature of rotor material is initially set to ambient which in this case is taken as 40 degrees Celsius. The temperature of powder and air were assigned the value of 300 and 80 degrees Celsius. These values represent typical operational conditions.

Convection Boundary Conditions:

At the left, right, and top surface of the rotor, where the rotor interfaces with powder and air

- For left surface (θ =0)

$$T_{new}(:,1,:) = T(:,2,:) + \left(\frac{dtheta * r_i * h_{phase}}{k_r}\right) * (T_{phase} - T(:,2,:) \quad (3.8)$$

- For right surface (θ =8mm)

$$T_{new}(:,end,:) = T(:,end-1,:) + \left(\frac{dtheta * r_i * h_{phase}}{k_r}\right) * (T_{phase} - T(:,end-1,:) \quad (3.9)$$

- For top surface (outer radius)

$$T_{new}(end,:,:) = T(end-1,:,:) + \left(\frac{dr * h_{phase}}{k_r}\right) * (T_{phase} - T(end-1,:,:) \quad (3.10)$$

- For bottom surface (inner radius)

$$T_{new}(1,:,:) = T(2,:,:) \quad (3.11)$$

- For front surface (z =0)

$$T_{new}(:,:,1) = T(:,:,2) + \left(\frac{dz * h_{phase}}{k_r}\right) * (T_{phase} - T(:,:,2)) \quad (3.12)$$

- For top surface (z = 0.330)

$$T_{new}(:,:,end) = T(:,:,end-1) + \left(\frac{dz * h_{phase}}{k_r}\right) * (T_{phase} - T(:,:,end-1) \quad (3.13)$$

Note: Here h_{phase} is representing convective heat transfer coefficient for air and powder phase (i.e., when rotor is in powder contact it is representing powder heat transfer coefficient and when it is in air representing air heat transfer coefficient).

Isothermal Boundary Conditions:

We have assumed that there will be no heat transfer from the shaft to the blade at their interface as both are at the same temperature. We are assuming the same temperature considering that both the rotor blade and rotor shaft surface exposed to powder are getting heated at the same rate and thus temperature rises with the same amount nullifying any temperature gradient.

Temporal Boundary Conditions:

The temperature distribution of each pocket is updated based on the heat transfer and boundary condition applied at each time step.

3.6 Numerical Method Used

The numerical method used for solving the transient heat conduction equation in two dimensions is based on the finite difference technique, which gives the evolution of temperature in the rotor over time. The heat conduction equation in two dimensions is expressed as:

$$\frac{\partial T(r,\theta,z,t)}{\partial t} = \alpha\left(\frac{1}{r}\frac{\partial}{\partial r}\left(r\frac{\partial T(r,\theta,z,t)}{\partial r}\right) + \frac{1}{r^2}\frac{\partial^2 T(r,\theta,z,t)}{\partial \theta^2} + \frac{\partial^2 T(r,\theta,z,t)}{\partial z^2}\right) \quad (3.14)$$

where: $\boldsymbol{T(r,\theta,z,t)}$ represents the temperature distribution across the spatial coordinate and time. α

represents the thermal diffusivity of the material.$\frac{\mathbf{1}}{\boldsymbol{r}}\frac{\boldsymbol{\partial}}{\boldsymbol{\partial r}}\left(\boldsymbol{r}\frac{\boldsymbol{\partial T(r,\theta,z,t)}}{\boldsymbol{\partial r}}\right)$ representing the conduction in the radial direction. The term r appears because of the geometry of the cylinder and handles the variation as we move outward radially.$\frac{\mathbf{1}}{\boldsymbol{r^2}}\frac{\boldsymbol{\partial^2 T(r,\theta,z,t)}}{\boldsymbol{\partial\theta^2}}$ represent the variation of temperature in the circumferential direction. The term $\boldsymbol{r^2}$ in the denominator is there because of the geometry. $\frac{\boldsymbol{\partial^2 T(r,\theta,z,t)}}{\boldsymbol{\partial z^2}}$, this term accounts for the temperature variation along the axial direction z, where heat is conducted along the length of the cylinder.

Spatial and Temporal Discretization

To apply the finite difference method, we have discretized the spatial and time domain as follows:

- *Radial Discretization:* The radial grid is divided into nr grid points and the space between the two radial grid points is obtained as:

$$\partial r = \frac{(r\_outer - r\_inner)}{nr - 1} \tag{3.15}$$

The radial coordinate for each grid point 'i' is given by:

$$r\_i = r\_inner + (i - 1) * \partial r \tag{3.16}$$

where 'i' ranges from 1 to nr.

- *Circumferential Discretization:* The circumferential domain is divided into nθ grid points and the spacing between to points in the circumferential direction is given as:

$$\partial\theta = \frac{r\_outer * \theta_{pocket}}{n\theta} \tag{3.17}$$

The circumferential coordinate θ_j for each grid point, j is expressed as:

$$\theta_j = j.\partial\theta \tag{3.18}$$

where j varies from 0 to $n\theta - 1$.

- *Axial Discretization:* The axial domain is divided into nz grid points, with the spacing between two grid points in the axial direction given by:

$$\partial z = \frac{Axial\ Length}{nz - 1} \tag{3.19}$$

The axial coordinate z_k for each grid point 'k' is given by:

$$z_k = (k - 1) * \partial z \tag{3.20}$$

where 'k' ranges from 1 to nz.

- *Temporal Discretization:* The time domain is discretized as ----

$$t_n = n.\Delta t, where\ n = 0,1,2,\ldots\ldots \quad (3.21)$$

Where, Δt is representing the timestep and n represents the time step.

3.7 Finite difference approximation:

We are approximating/ discretizing the spatial and temporal derivatives using Finite difference method.

- *Time derivatives:* The time derivative at the nth time interval is obtained using the forward difference method.

$$\left(\frac{\partial T}{\partial t}\right)_{(\mathrm{r_i},\theta_j,n_k)} \approx \frac{T_{i,j,k}^{n+1} - T_{i,j,k}^{n}}{\Delta t} \quad (3.22)$$

The method is called forward difference as it uses the value at the point ahead of the initial position to approximate the derivative.

- *Radial derivatives:* The radial derivative is discretized using a central differencing scheme using grid points $(\mathrm{r_i}, \theta_j, n_k)$.

$$\left(\frac{\partial^2 T}{\partial r^2}\right)_{(\mathrm{r_i},\theta_j,n_k)} \approx \frac{T_{i+1,j,k}^{n} - 2T_{i,j,k}^{n} + T_{i-1,j,k}^{n}}{\Delta r^2} \quad (3.23)$$

The term $\frac{1}{r}\frac{\partial}{\partial r}\left(r\frac{\partial T}{\partial r}\right)$ is approximated as:

$$\frac{1}{r_i}\frac{\partial}{\partial r}\left(r_i\frac{\partial T}{\partial r}\right) \approx \frac{1}{r_i}\left(\frac{r_{i+1}T_{i+1,j,k}^{n} - r_{i-1}T_{i-1,j,k}^{n}}{2\Delta r}\right) \quad (3.24)$$

The central difference scheme of derivative approximation is the most accurate one as it considers both forward and backward schemes. It uses the neighboring value (forward and backward point value) to approximate the derivative.

- *Circumferential derivatives:* It is also approximated using a central difference scheme at the grid point $(\mathrm{r_i}, \theta_j, n_k)$.

$$\left(\frac{\partial^2 T}{\partial \theta^2}\right)_{(\mathrm{r_i},\theta_j,n_k)} \approx \frac{T_{i,j+1,\mathrm{k}}^{n} - 2T_{i,j,k}^{n} + T_{i,j-1,\mathrm{k}}^{n}}{\Delta \theta^2} \quad (3.25)$$

- *Axial derivatives:* It is also approximated using a central difference scheme at the grid point $(\mathrm{r_i}, \theta_j, n_k)$.

$$\left(\frac{\partial^2 T}{\partial z^2}\right)_{(\mathrm{r_i},\theta_j,n_k)} \approx \frac{T_{i,j,k+1}^{n} - 2T_{i,j,k}^{n} + T_{i,j,k-1}^{n}}{\Delta z^2} \quad (3.26)$$

Explicit and implicit method:

There are two famous approaches to solving discretized heat conduction equations: explicit and implicit methods. Each method has its advantages and limitations.

- *Implicit method:* In this method, the temperature at the next timestep is dependent on both current and next timestep temperature values. This method involves solving several equations at each timestep which makes computation difficult but despite this, it is unconditionally stable for any time step.

- *Explicit method:* This method is based on updating temperature in the future time step based on the value of temperature at the current time step. We get the following expression when we integrate the finite difference approximation and heat conduction equation.

$$\boldsymbol{T_{i,j,k}^{n+1}} = \boldsymbol{T_{i,j,k}^{n}} + \propto . \Delta t \left(\frac{1}{r_i} \left(\frac{r_{i+1} T_{i+1,j,k}^{n} - r_{i-1} T_{i-1,j,k}^{n}}{2\Delta r} \right) + \frac{T_{i,j+1,\mathrm{k}}^{n} - 2T_{i,j,k}^{n} + T_{i,j-1,\mathrm{k}}^{n}}{\Delta \theta^2} + \frac{T_{i,j,\mathrm{k}+1}^{n} - 2T_{i,j,k}^{n} + T_{i,j,\mathrm{k}-1}^{n}}{\Delta z^2} \right) \quad (3.27)$$

This method is very simple to implement but comes with restrictions to satisfy stability criteria like CFL condition (Courant-Friedrichs-Lewy condition) to maintain numerical stability. These conditions limit the time step size and thus make it computationally expensive for fine grids or highly conductive materials.

Rationale for Explicit Method:

- Simplicity and Implementation: This method is easy to implement as it directly updates the temperature based on the previously known value.

- Computational Efficiency: Allowing for quick iterations and rapid convergence towards a solution for relatively small systems and time steps, and it is computationally less intensive for small systems.

- Physical Interpretation: This method gives an easy way of understanding the evolution of temperature with time, as each time step is calculated based on the immediately preceding state.

Scheme and Algorithm for Explicit Method

- Initialization:
- Boundary conditions:
- Time Stepping Loop:
- Convergence:
- Output

Stability and Time Step Selection

It has been known that the stability of a numerical method is dependent on the value of stability criteria defined as----

$$\propto . \Delta t \left(\frac{1}{(\Delta r^2)} + \frac{1}{(\Delta \theta^2)} + \frac{1}{(\Delta z^2)} \right) \leq \frac{1}{2} \quad (3.28)$$

This condition restricts the maximum allowable size of the time step.

CHAPTER 4: Results and Discussion

4.1 Overview

This section discusses the detailed interpretation of the results of the thermal behavior analysis of the rotary airlock valve, coined from the simulation of the rotary valve rotor constructed using SS316 (stainless steel) and mild steel, typically under high-temperature industrial powder handling conditions. A 3D transient heat transfer model was developed and discretized in cylindrical coordinates, and a finite difference-based numerical solver was developed using MATLAB to capture the temperature distribution, material response to thermal loads, and operational parameters such as iteration count and time to equilibrium. Each rotor configuration was tested with two powder types, sand and ash. The results are presented in the context of tackling the major challenges incurred by rotary airlocks (RALs), such as thermal expansion, sealing loss, non-uniform heating, air leakage, fatigue, sintering, and heat transfer inefficiencies.

4.2 Simulations Insights and Numerical Behavior

Transient response and convergence: Initially, the system was at rest at 40°C. Upon operation, it was exposed to powders at 300°C and air at 80°C. The system is considered to have reached steady state once temperature changes fall below a threshold of 0.1°C. Simulations were conducted for a rotary airlock constructed from SS 316 and mild steel, handling two types of powders: sand and ash. Key simulation details—including the number of iterations to reach steady state, time required to achieve steady state, and the average pocket temperature—were recorded and are summarized in Table 4.1.

Table 4.1 Thermal Response Summary (SS316 & MS with Sand/Ash)

Metric	SS 316		Mild Steel	
	Sand	Ash	Sand	Ash
Steady-state iterations	95	97	77	79
Time to steady state (s)	285	291	231	237
Average pocket temp (°C).	295.1	295.35	295.45	295.26

The SS316 rotor (thermal conductivity, K = 16 W/m·K) reaches steady state more slowly than the mild steel rotor (K = 55 W/m·K) due to its lower thermal conductivity, which limits radial heat diffusion. This outcome is consistent with physical intuition and supports the credibility of the simulation model.

The choice of rotor material significantly impacts both thermal diffusivity (α) and heat storage capacity (ρCp), influencing the rate of temperature change and the material's ability to retain thermal energy.

- **SS316**: $\alpha \approx 4.08 \times 10^{-6}\ m^2/s$
- **Mild Steel**: $\alpha \approx 1.41 \times 10^{-5}\ m^2/s$

This marked difference explains why the mild steel rotor reaches steady state more rapidly. Conversely, the slower heat penetration in SS316 promotes a more uniform and stable thermal distribution, which can be beneficial in applications involving cyclic thermal loading.

4.3 Temperature Contour Visualization:

Three-dimensional temperature contour plots were generated to visualize the spatial temperature distribution across all rotor blades for different combinations of rotor materials and powders. The configurations studied include mild steel and SS316 rotors, each handling sand and ash powders. These plots were extracted after the 5th iteration, under transient conditions, before the system reached steady state. This allows for the examination of early-stage heat distribution and the identification of developing thermal gradients during system startup.

In the contour plots, the x-axis and y-axis represent spatial dimensions (i.e., radial and circumferential) (in meters), labeled as X (m) and Y (m), while the z-axis, labeled as Z (m), corresponds to the axial direction of the rotor. Temperature variation is depicted using a color-coded scale, ranging from dark blue (indicating the lowest temperatures, approximately 160 °C) to dark red (indicating the highest temperatures, approximately 280 °C), with intermediate colors showing smooth temperature transitions.

These visualizations provide important insights into how heat begins to propagate through the rotor assembly, highlighting the influence of material properties and powder type on early thermal response. This transient analysis serves as a foundation for understanding the system’s progression toward thermal equilibrium and supports further discussion on thermal design and material selection.

Mild Steel with sand

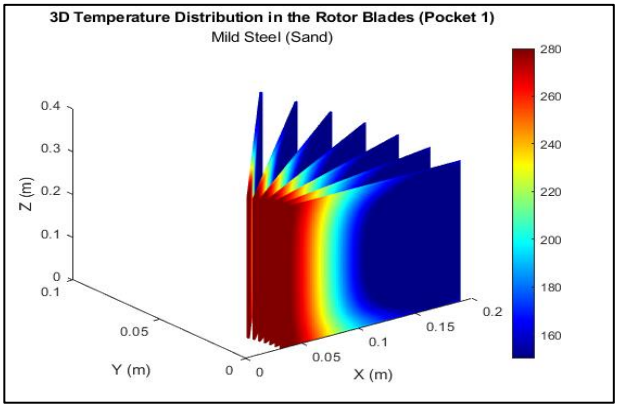

Figure 4.1 Temperature contour (MS + Sand) Blade 1 between pockets 10 & 1

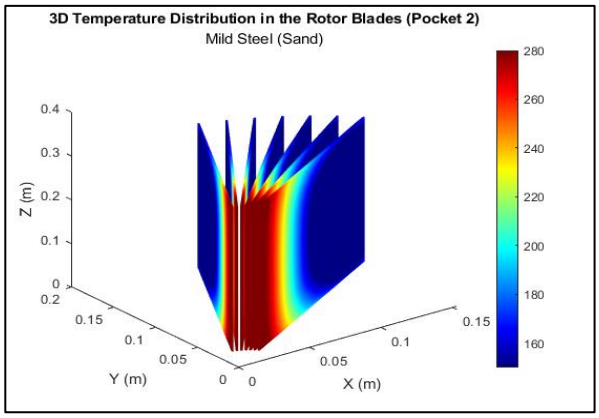

Figure 4.2 Temperature contour (MS +Sand) Blade 2 between pockets 1 & 2

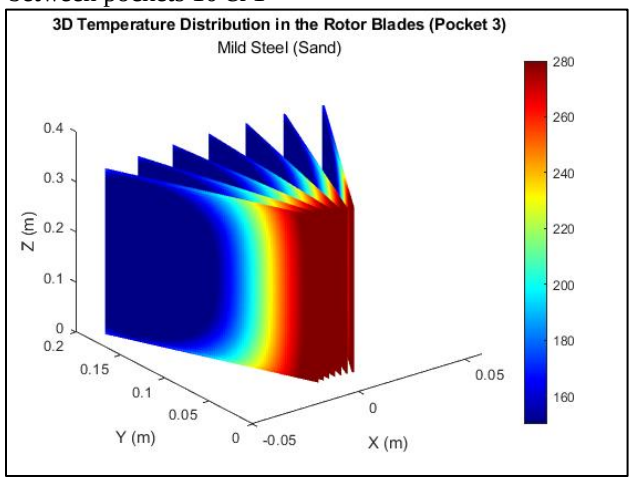

Figure 4.3 Temperature contour (MS + Sand) Blade 3 between pockets 2 & 3

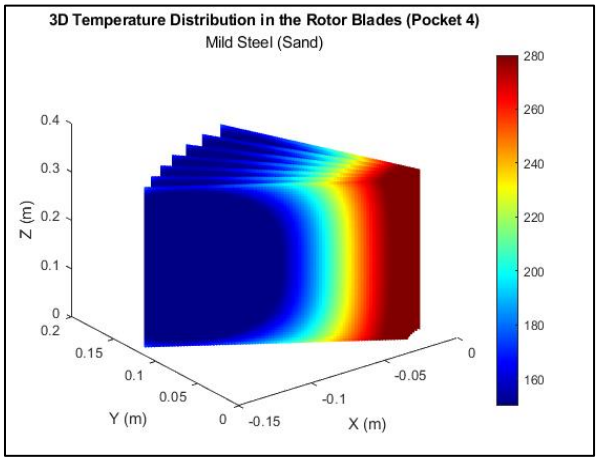

Figure 4.4 Temperature contour (MS + Sand) Blade 4 between pockets 3 & 4

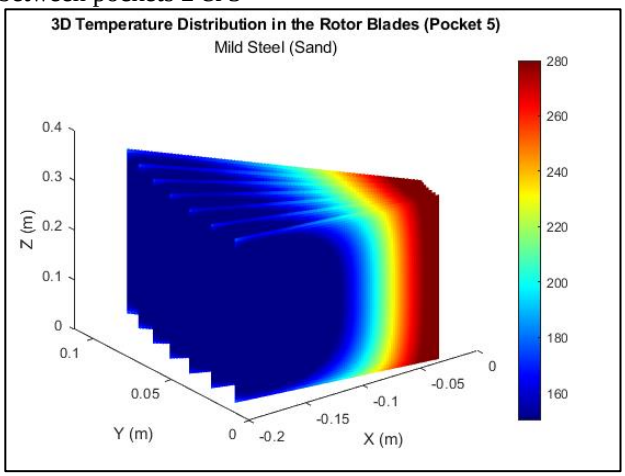

Figure 4.5 Temperature contour (MS + Sand) Blade 5 between pockets 4 & 5

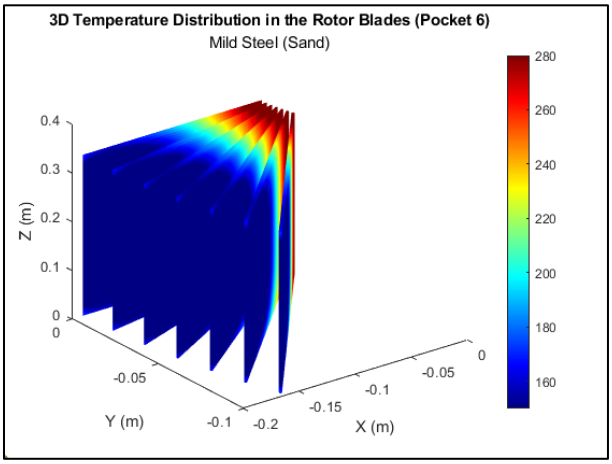

Figure 4.6 Temperature contour (MS +Sand) Blade 6 between pockets 5 & 6

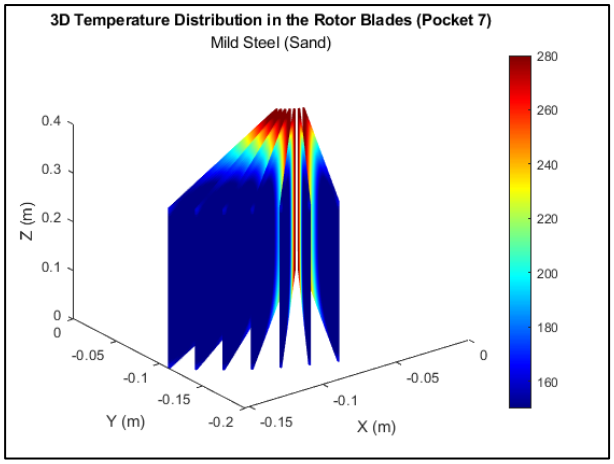

Figure 4.7 Temperature contour (MS + Sand) Blade 7 between pockets 6 & 7

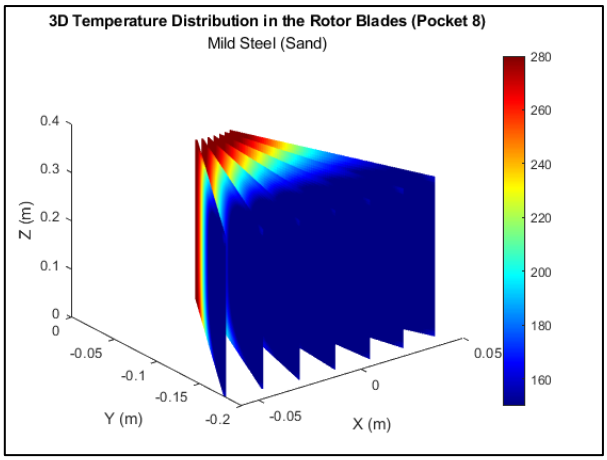

Figure 4.8 Temperature contour (MS + Sand) Blade 8 between pockets 7 & 8

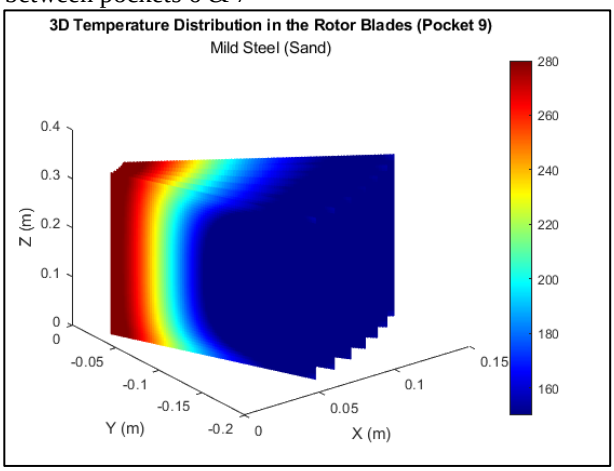

Figure 4.9 Temperature contour (MS + Sand) Blade 9 between pockets 8 & 9

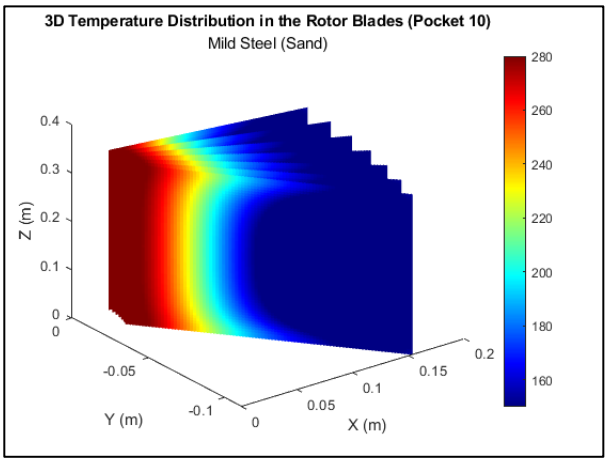

Figure 4.10 Temperature contour (MS + Sand) Blade 10 between pockets 9 & 10

In the mild steel rotor exposed to sand, Figures 4.1 through 4.10 depict a progressive and non-uniform radial heat propagation from Blade 1 through blade 10. As the Blades 1 to 4 comes into contact with sand earlier and remain in contact longer, it is evident that they attain higher temperature compared to the remaining Blades, with recorded values ranging from approximately **172.2°C** to **174.1°C** as noted in Table 4.4.

From Blade 5 (Figures 4.10), onward, heat distribution becomes relatively uniform, particularly noticeable in Blades 6 and 7. The figure indicate that the hotter zone band gradually diminishes from Blade 5 to 9 (Figures 4.5 to 4.9). This can be attributed to the Blades having already discharged the powder and now beginning to lose heat, primarily through convection exchange with air, leaking during the return rotation.

In Blade 10 (Figures 4.10), a slight increase in thermal intensity is observed. This is consistent with the Blade's re-entry into the powder feeding zone, where it progressively absorbs heat through renewed contact with the hot particulate material.

Mild Steel with Ash

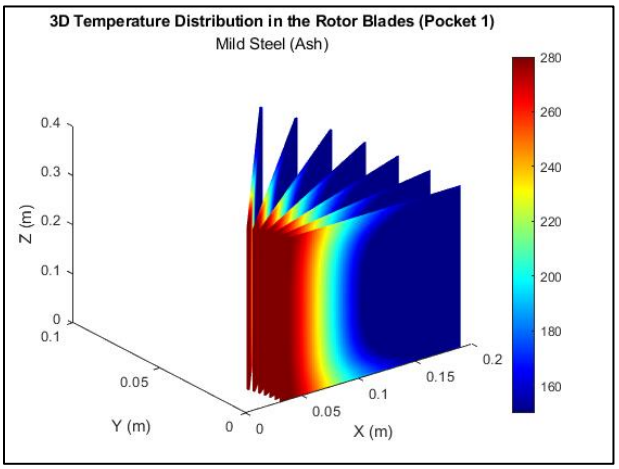

Figure 4.11 Temperature contour (MS + Ash) Blade 1 between pockets 10 & 1

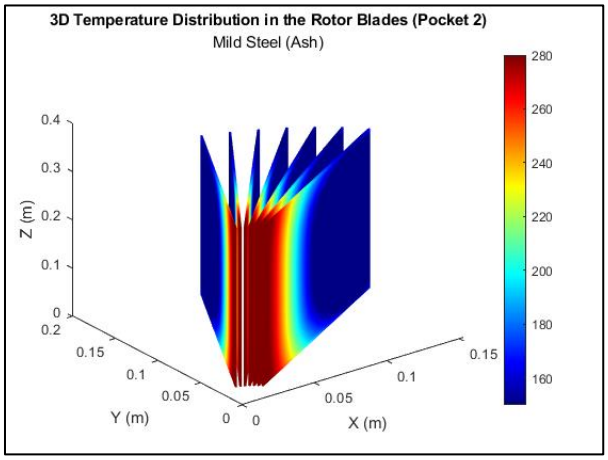

Figure 4.12 Temperature contour (MS + Ash) Blade 2 between pockets 1 & 2

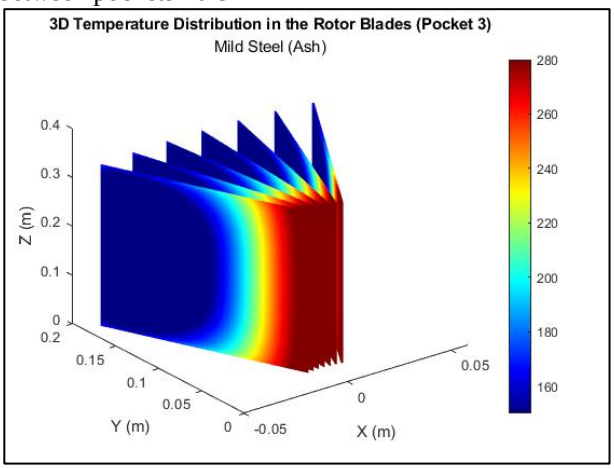

Figure 4.13 Temperature contour (MS + Ash) Blade 3 between pockets 2 & 3

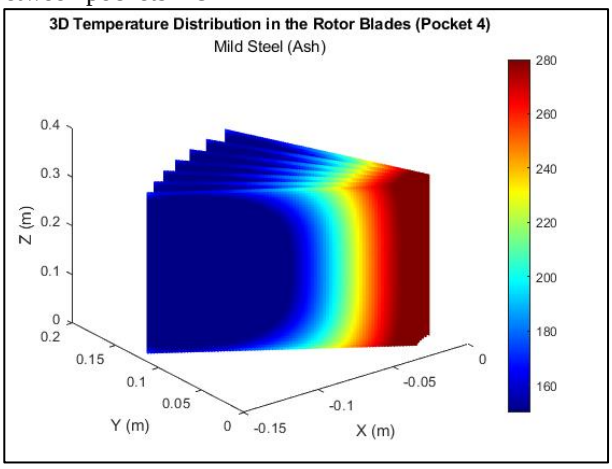

Figure 4.14 Temperature contour (MS + Ash) Blade 4 between pockets 3 & 4

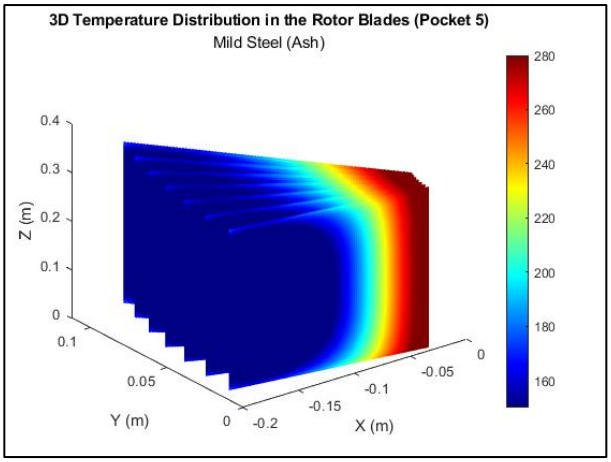

Figure 4.15 Temperature cotour (MS + Ash) Blade 5 between pockets 4 & 5

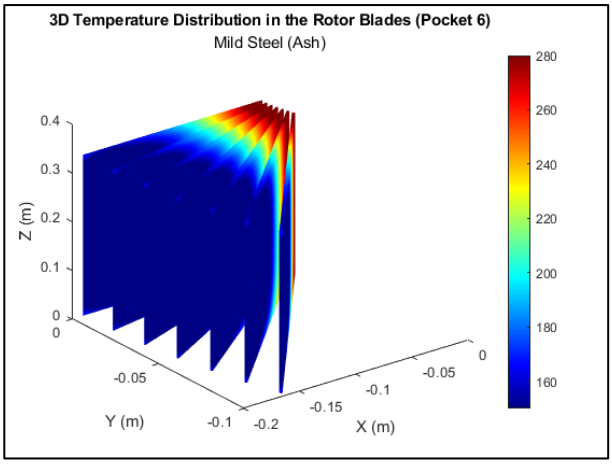

Figure 4.16 Temperature contour (MS + Ash) Blade 6 between pockets 5 & 6

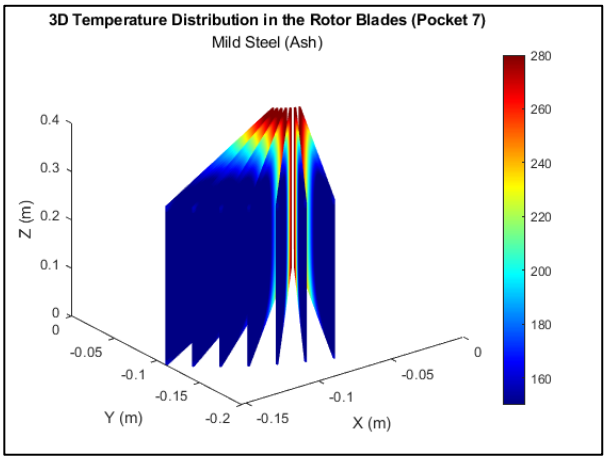

Figure 4.17 Temperature cotour (MS + Ash) Blade 7 between pockets 6 & 7

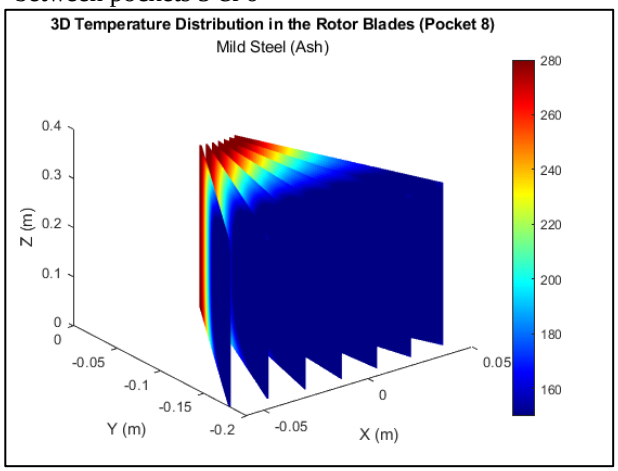

Figure 4.18 Temperature contour (MS + Ash) Blade 8 between pockets 7 & 8

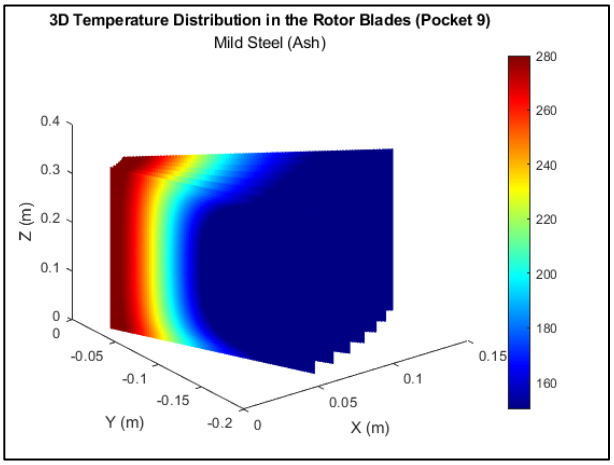

Figure 4.19 Temperature contour (MS + Ash) Blade 9 between pockets 8 & 9

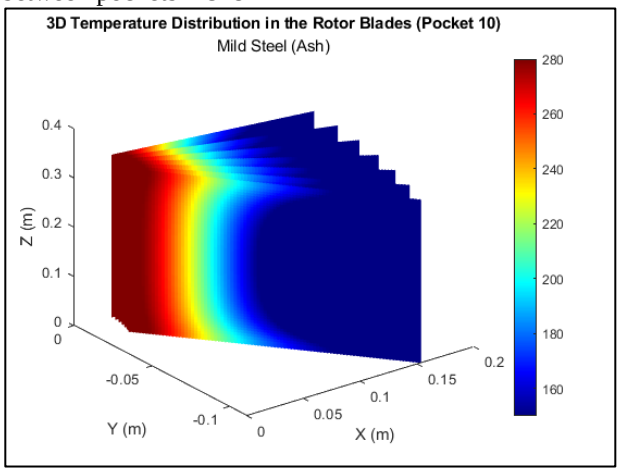

Figure 4.20 Temperature contour (MS + Ash) Blade 10 between pockets 9 & 10

For mild steel with ash, the temperature range observed after the same number of iterations is lower than that in the case of sand. As seen in Figures 4.11 to 4.14, Blades 1 to 4 show a similar heating pattern as shown in mild steel with sand but with reduced radial penetration and overall lower intensity. The maximum temperatures in this range are approximately **171.5°C**, while the minimum is around **169.6°C**, as listed in Table 4.5. The behavior is due to ash's lower thermal conductivity, which moderates the heating rate and leads to lower peak temperatures.

From Blades 5 to 9 (Figures 4.15 to 4.19), the temperature contours exhibit more evenly distributed heat, with no sharp gradients, confirming ash's role as a thermal buffer. The higher specific heat and insulating nature of ash help to stabilize temperature over time and reduce thermal shocks. These Blades also display a narrower band of high-temperature zones, owing to convective heat loss during the return cycle.

At Blade 10 (Figures 4.20), a renewed temperature increase is observed. This is attributed to recontact with hot powder, initiating a fresh heating phase similar to that seen in Blade 1.

SS316 with Sand

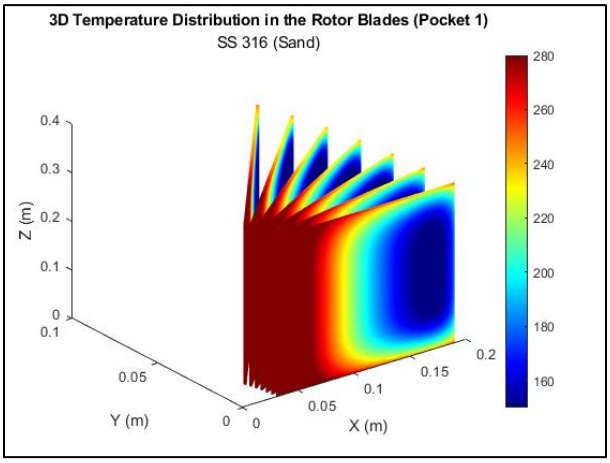

Figure 4.21 Temperature contour (SS316 +Sand) Blade 1 between blades 10 & 1

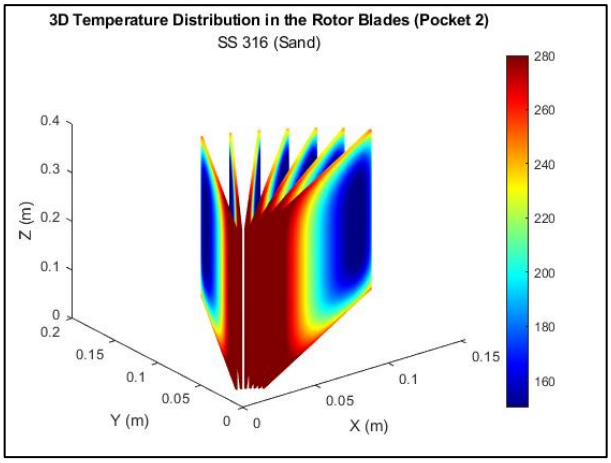

Figure 4.22 Temperature contour (SS316 +Sand) Blade 2 between pockets 1 & 2

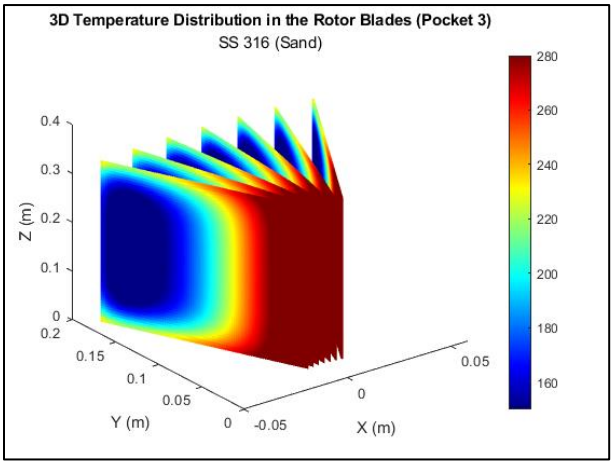

Figure 4.23 Temperature contour (SS316 +Sand) Blade 3 between pockets 2 & 3

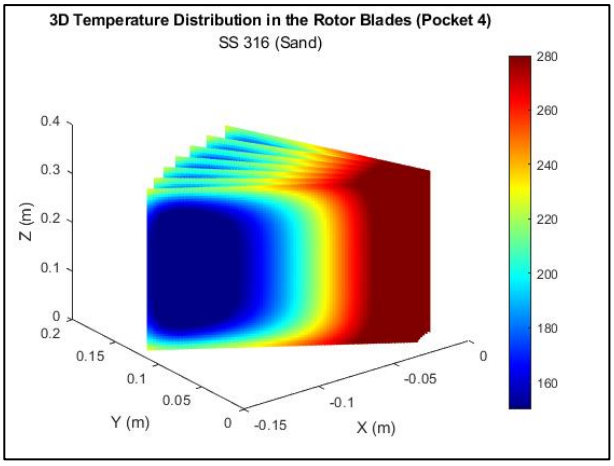

Figure 4.24 Temperature contour (SS316 +Sand) Blade 4 between pockets 3 & 4

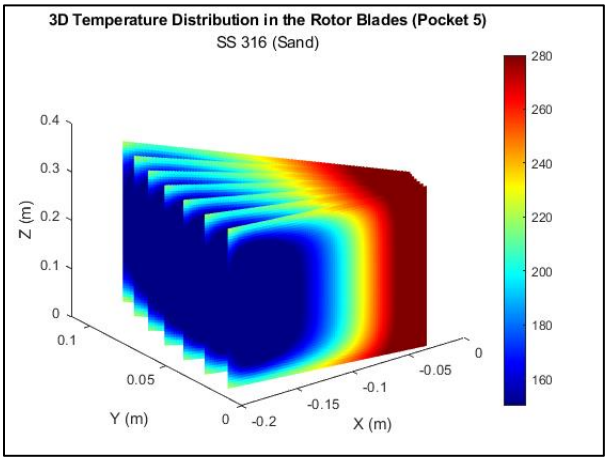

Figure 4.25 Temperature contour (SS316 +Sand) Blade 5 between pockets 4 & 5

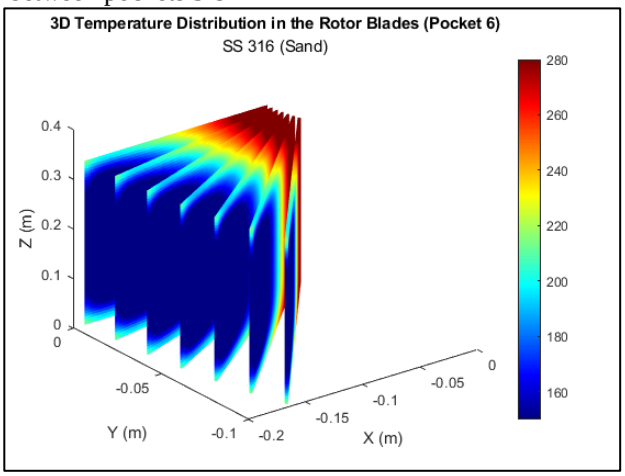

Figure 4.26 Temperature contour (SS316 +Sand) Blade 6 between pockets 5 & 6

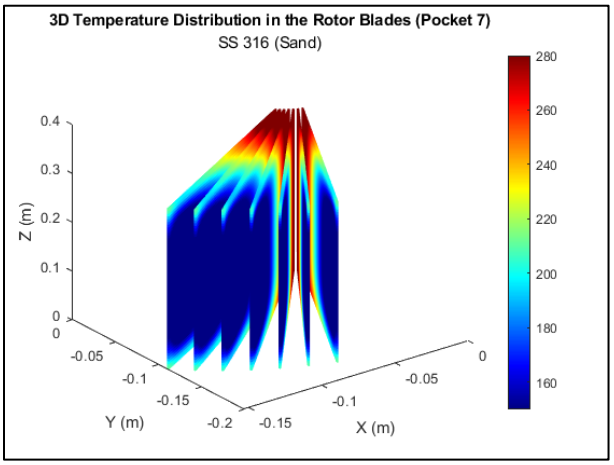

Figure 4.27 Temperature contour (SS316 +Sand) Blade 7 between pockets 6 & 7

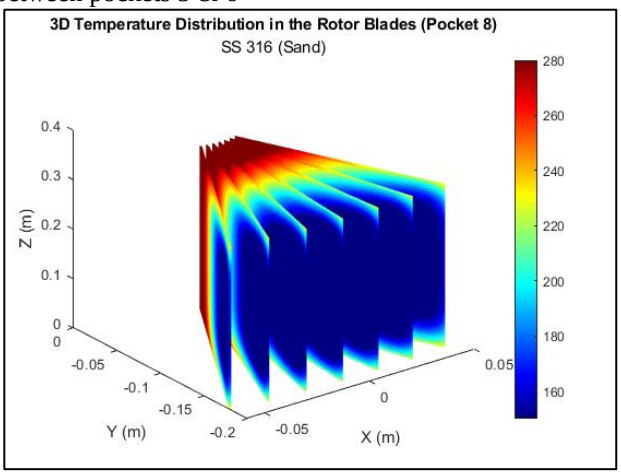

Figure 4.28 Temperature contour (SS316 +Sand) Blade 8 between pockets 7 & 8

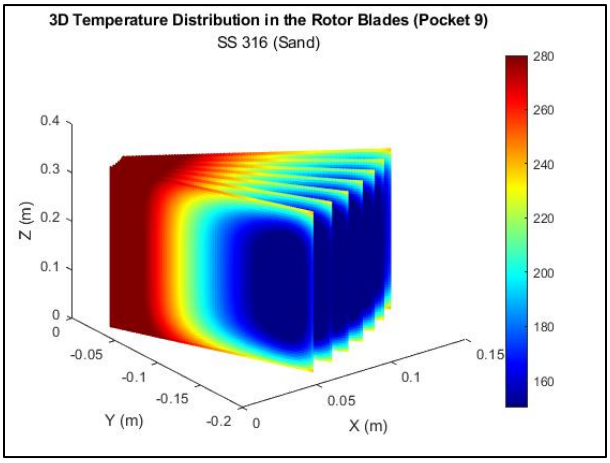

Figure 4.29 Temperature contour (SS316 +Sand) Blade 9 between pockets 8 & 9

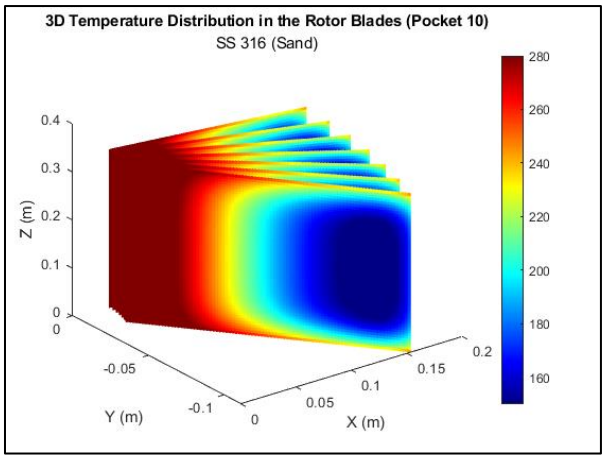

Figure 4.30 Temperature contour (SS316 +Sand) Blade 10 between pockets 10 & 1

SS316's lower thermal conductivity is evident in Figures 4.21 to 4.30, where heat retention is dominant, particularly in the axial and radial base regions of each blade. In Blades 1 to 4, heat accumulates primarily near the blade root, resulting in localized axial hotspots. The thermal spread is limited in the radial direction, which differs significantly from the mild steel case.

According to Table 4.6, temperatures in this phase range from **211.7°C** to **215.8°C**, indicating higher thermal storage across the blade material. Due to SS316's slower heat conduction, a lag in heat propagation is observed, but it helps in forming a more stable axial heat field over time.

Blades 5 to 9 (Figures 4.35 to 4.39), begin to exhibit thermal symmetry, although the base temperatures remain relatively high. Notably, the extent of the hottest zone narrows in this region, implying that SS316 starts stabilizing its heat profile with less surface area at peak temperature than in Blades 1 to 4. This stabilization improves resistance to fatigue and thermal deformation.

In Blade 10 (Figure 4.30), the thermal profile begins to rise again, resembling the heating patterns seen in the early blades. This occurs due to its re-engagement with hot powder, initiating the next heating cycle.

SS316 with Ash

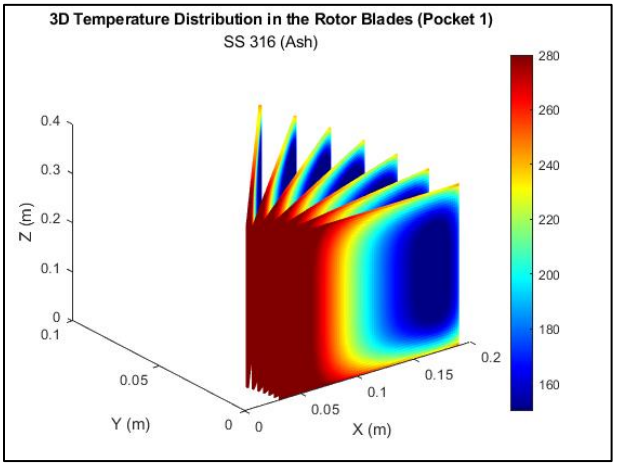

Figure 4.31 Temperature contour (SS316 +Ash) Blade 1 between pockets 10 & 1

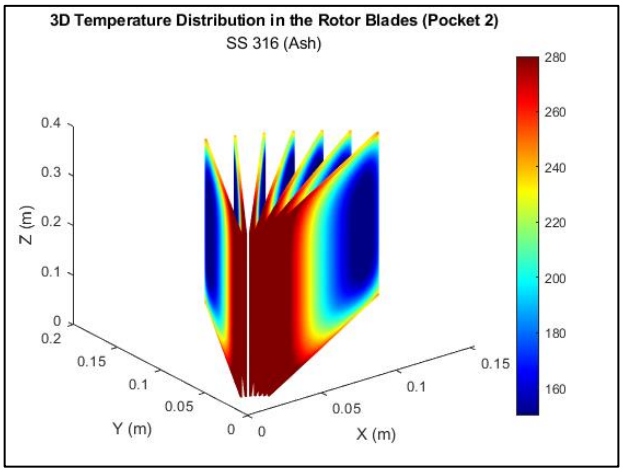

Figure 4.32 Temperature contour (SS316 +Ash) Blade 2 between blades 1 & 2

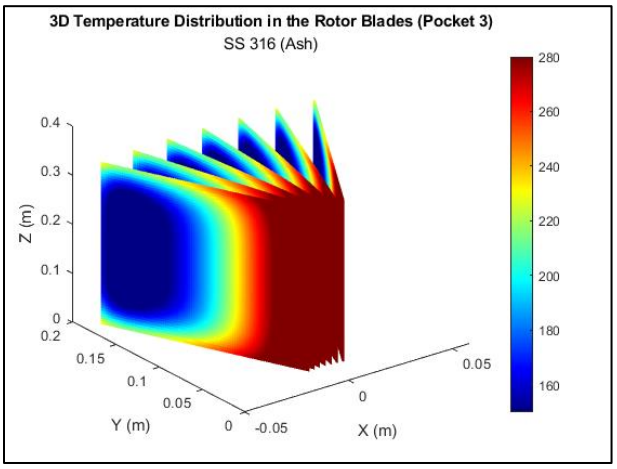

Figure 4.33 Temperature contour (SS316 +Ash) Blade 3 between pockets 2 & 3

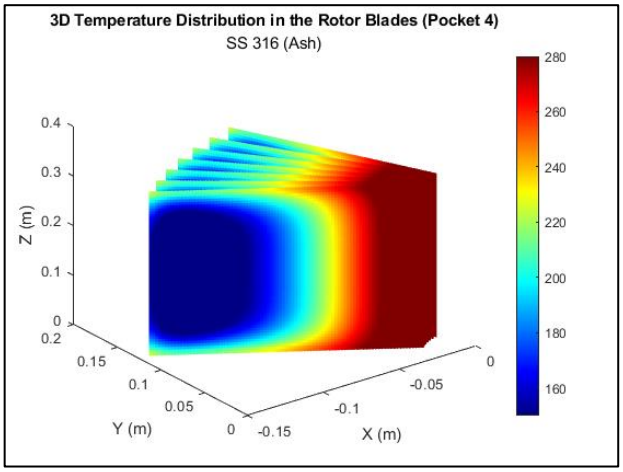

Figure 4.34 Temperature contour (SS316 +Ash) Blade 4 between pockets 3 & 4

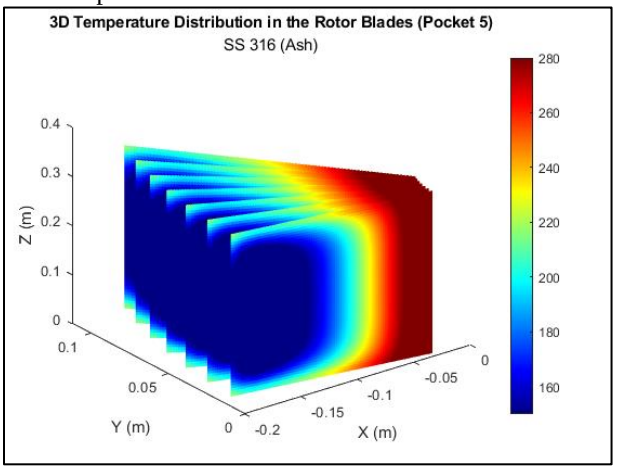

Figure 4.35 Temperature cotour (SS316 +Ash) Blade 5 between pockets 4 & 5

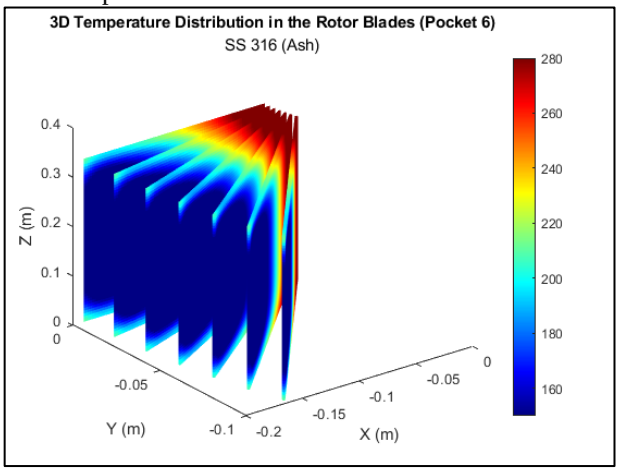

Figure 4.36 Temperature contour (SS316 +Ash) Blade 6 between pockets 5 & 6

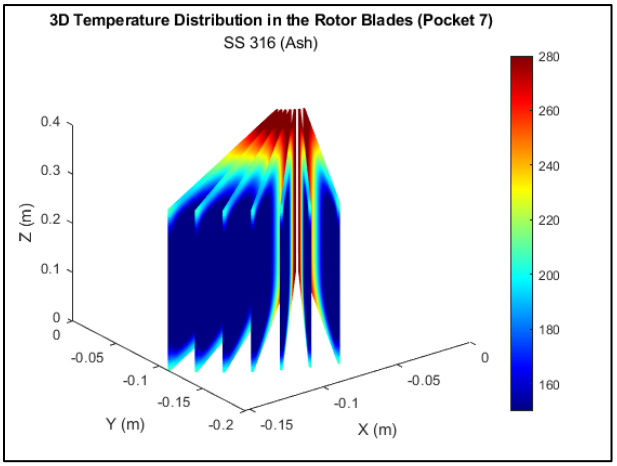

Figure 4.37 Temperature contour (SS316 +Ash) Blade 7 between pockets 6 & 7

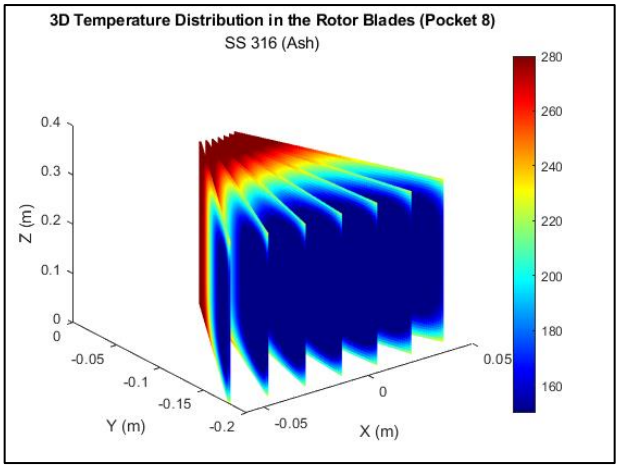

Figure 4.38 Temperature contour (SS316 +Ash) Blade 8 between pockets 7 & 8

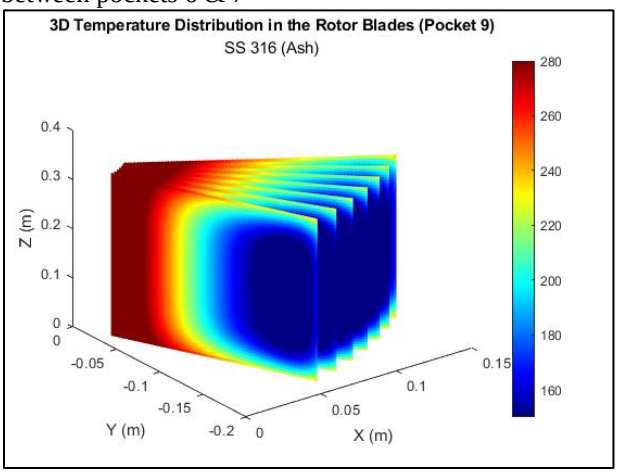

Figure 4.39 Temperature contour (SS316 +Ash) Blade 9 between pockets 8 & 9

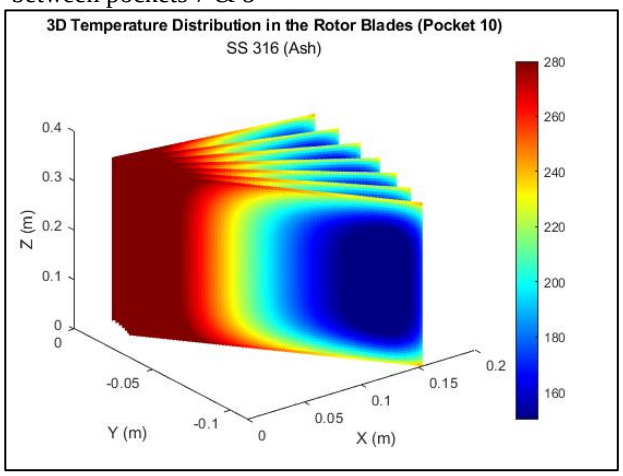

Figure 4.40 Temperature contour (SS316 +Ash) Blade 10 between blades 9 & 10

In the SS316 rotor with ash, the temperature distribution follows a pattern similar to other cases but with notable distinctions driven by the combined low thermal conductivity of both SS316 and ash.

Figures 4.31 to 4.34 (Blades 1 to 4) show a non-uniform heating pattern, where temperature buildup is localized, and significant asymmetry is visible across both radial and axial sections. Heat is not evenly distributed across the blade face, resulting in hotspots clustered near the shaft and blade edges. This reflects a slow and spatially inconsistent heat absorption phase due to SS316's thermal inertia and ash's insulating nature.

Between Blades 5 and 9 (Figures 4.35 to 4.39), the temperature field becomes more stabilized, and a narrower band of the hottest zone is observed compared to Blades 1–4. This suggests that after discharging the powder, the blades begin to lose heat via convection to the surrounding air. The sharper drop-off in high-temperature zones is also a result of leakage paths and flow exposure on the return

side of the rotation cycle.

In Blade 10 (Figure 4.40), the temperature begins to rise again, reflecting its reintroduction into the powder feeding zone. This heating pattern mimics that of the early blades, initiating a new cycle of thermal loading as the blade receives hot particles once more.

As per Table 4.7, the temperature in this configuration ranges from **209.2°C** to **212.8 °C**, supporting the observation of subdued heating with significant retention—a characteristic of both the material and powder phase used.

4.4 Thermal Expansion and Clearance Loss

One of the most critical challenges in the operation of rotary airlock valves (RALs) is the reduction of clearance between the rotor and housing due to thermal expansion. The numerical simulation effectively captured the time-dependent, three-dimensional temperature distribution, which directly correlates with the material's expansion potential. Owing to its higher thermal conductivity, mild steel reaches thermal equilibrium more quickly than SS316, but this also increases the risk of thermal expansion and consequent clearance reduction—unless appropriately accounted for in the design. In contrast, SS316 exhibits a slower and more controlled thermal response, minimizing the likelihood of abrupt or excessive expansion. To quantitatively assess thermal expansion, the linear thermal expansion formula is applied.

Where:

ΔL = expansion length

α = coefficient of linear thermal expansion

L_0= original length

ΔT = change in temperature

Assuming a radial length L_0= 0.16m (outer to inner radius difference) and maximum ΔT = 256°C, we get:

SS316 ($\alpha = 17.2 \times 10^{-6}$): $\Delta L_{ss316} = 0.705$ mm

Mild Steel ($\alpha = 13.5 \times 10^{-6}$): $\Delta L_{ss316} = 0.553$ mm

Despite its faster heating rate, mild steel undergoes slightly less thermal expansion than SS316 due to its lower coefficient of thermal expansion. However, the more abrupt rate of temperature change in mild steel may elevate the risk of dynamic clearance issues during operation. These findings underscore the importance of incorporating precise thermal allowances in rotor-to-housing design to ensure reliable performance under varying thermal conditions.

4.5 Non-Uniform Temperature Distribution

The study also reveals the presence of axial and circumferential temperature gradients, particularly in SS316 rotors. The 3D contour plots indicate that the central region and axial ends tend to reach the highest temperatures, while circumferential zones in contact with the powder phase are heated more than those exposed to air. These temperature gradients induce mechanical stresses that can potentially affect the alignment and performance of rotor vanes. The slower radial heat conduction in SS316 contributes to more pronounced thermal non-uniformity, highlighting the importance of structural considerations—such as adopting symmetric designs and exploring the use of gradient-tolerant alloysto mitigate thermal distortion.

4.6 Air Leakage and Pressure Loss

Pressure integrity is a critical factor in the performance of pneumatic conveying systems. Thermal flux-induced deformation can compromise this integrity, leading to air leakage. Analysis of pocket temperatures over time revealed that pockets transitioning from powder to air phases exhibited a slight but consistent delay in cooling, indicating potential leakage zones. Mild steel, owing to its faster thermal equilibration, maintained more uniform sealing performance throughout rotation. These findings suggest that SS316 rotors, due to their slower thermal contraction, may benefit from flexible or adaptive sealing mechanisms designed to accommodate transient thermal gradients and ensure sustained pressure integrity.

4.7 Sintering and Powder Stickiness

Handling materials such as ash involves a risk of sintering, particularly when the rotor surface retains elevated temperatures after discharge. The study indicates that SS316, due to its lower thermal conductivity, retains more heat in the rotor body. While this thermal inertia contributes to process

stability and smoother thermal transitions, it also increases the risk of ash sintering on the rotor surface. In contrast, mild steel cools more rapidly, which helps mitigate sintering risks but may lead to greater thermal fluctuations. Consequently, when using SS316 with sticky or sinter-prone powders, surface treatments or coatings—such as Teflon or ceramic layers—may be necessary to reduce material adhesion and enhance rotor longevity.

4.8 Comparative Numerical Analysis

To provide a quantitative perspective, the table below summarizes key thermal performance metrics observed across all simulation scenarios:

Table 4.2 Performance Metrics Comparison

Rotor Material	Powder Type	Iterations to Steady State	Time to Steady State (s)	Average Pocket Temp. (°C)	Maximum Temp. Diff (°C)
SS316	Sand	95	285	295.5	0.8
SS316	Ash	97	291	295.4	0.7
Mild Steel	Sand	77	231	295.5	0.5
Mild Steel	Ash	79	237	295.3	0.4

Interpretation:

- **Mild steel** consistently required fewer iterations and reached thermal equilibrium more quickly, owing to its higher thermal conductivity.
- **SS316** exhibited slightly higher peak temperatures and greater temperature differentials, suggesting a higher potential for localized overheating.
- **Ash,** due to its lower bulk density and thermal conductivity, caused a slight delay in reaching thermal equilibrium in both rotor materials.

4.9 Material Trade-Offs and Operational Suitability

The choice between SS316 and mild steel should be guided by specific operational requirements:

- **SS316** provides superior corrosion resistance, enhanced fatigue life, and effective thermal buffering. However, it is prone to sintering issues and requires longer warm-up times due to slower heat conduction.
- **Mild steel** offers a faster thermal response and improved sealing consistency but is more vulnerable to wear and corrosion in harsh environments.

- This simulation-driven analysis supports data-informed decisions in material selection, design optimization, and operational safety for rotary airlock valves (RALs) operating in high-temperature powder handling applications.

Table 4.3 Recommendations for Rotor Material Selection in Thermal Environments

Challenge	Simulation Insight	Material Recommendation
Clearance Loss	Faster expansion in mild steel	Favor SS316 with thermal buffer
Thermal Gradient	SS316 shows hotspots	Use symmetric geometry, consider mild steel
Air Leakage	More sealing variance in SS316	Adaptive seals for SS316
Fatigue	Stable cycle in SS316	SS316 for fatigue resistance
Sintering	Higher residual temp in SS316	Coatings or MS for ash
Heat Transfer	Lag in the SS inner shaft	Fin/blade design optimization

This comprehensive discussion of results validates the simulation approach as a practical and reliable tool for evaluating and optimizing the thermal performance of rotary airlock valves under high-temperature industrial conditions.

4.10 Transient Thermal Behavior: Case-wise Analysis

Mild Steel with Sand:

Mild Steel with Sand display rapid and uniform heating from the outer edge to the inward. From table no. 3, it has been clearly observed that there is a progressive heating pattern during the transient phase and peaking near mid-section (at pocket 5) and then symmetrically tapering down. Thermal expansion rises up to ~0.3mm observed by 5 iterations. Blades show consistent outer radial temperature dominance & clearance reduction happens early but stabilizes quickly. It has been also observed that, the value of temperature at steady state from Pocket 1 to 10 is 295 degrees and the temperature after 5th iteration lies in the range from 172 to 174 degrees approx.

Table 4.4 Transient Temperature Distribution in Rotor Blades (MS + Sand)

Blades No.	Temperature at Steady State (°C)	Temperature After 5th Iteration (°C)
Blade 1	295.3	174.1
Blade 2	295.4	174.2
Blade 3	295.5	174.5
Blade 4	295.6	174.7
Blade 5	295.7	174.8
Blade 6	295.6	172.9
Blade 7	295.5	172.8

Blade 8	295.4	172.5
Blade 9	295.3	172.3
Blade 10	295.2	172.2

Mild Steel with Ash:

Mild Steel with fly ash displays slower heating rate along with milder thermal gradient due to lower thermal conductivity of ash. Initial heating shows a lower gradient than MS-Sand. It has been noticed that the overall thermal transient is smoother due to dampening effect of ash. Thermal expansion up to ~0.25mm observed by 5 iterations. It has been also observed that, the value of temperature at steady state from Pocket 1 to 10 is 295 degrees and the temperature after 5th iteration lies in the range from 169 to 172 degrees approx.

Table 4.5 Transient Temperature Distribution in Rotor Blades (MS + Ash)

Blades No.	Temperature at Steady State (°C)	Temperature After 5th Iteration (°C)
Blade 1	295.1	171.5
Blade 2	295.2	171.6
Blade 3	295.3	171.9
Blade 4	295.4	172.1
Blade 5	295.5	172.2
Blade 6	295.4	170.3
Blade 7	295.3	170.2
Blade 8	295.2	169.9
Blade 9	295.1	169.7
Blade 10	295.1	169.6

SS 316 with Sand:

Mild Steel with fly ash displays slower heating rate along with milder thermal gradient due to lower thermal conductivity of ash. Initial heating shows a lower gradient than MS-Sand. It has been noticed that the overall thermal transient is smoother due to dampening effect of ash. Thermal expansion up to ~0.25mm observed by 5 iterations. It has been also observed that, the value of temperature at steady state from Pocket 1 to 10 is 295 degrees and the temperature after 5th iteration lies in the range from 169 to 172 degrees approx.

Table 4.6 Transient Temperature Distribution in Rotor Blades (SS316 + Sand)

Blades No.	Temperature at Steady State (°C)	Temperature After 5th Iteration (°C)
Blade 1	295.5	215.8
Blade 2	295.6	215.5
Blade 3	295.7	210.5
Blade 4	295.8	206.5
Blade 5	295.9	202.3
Blade 6	295.5	197.7
Blade 7	295.5	197.4
Blade 8	295.3	203.4
Blade 9	295.2	207.8
Blade 10	295.1	211.7

SS 316 with Ash:

Mild Steel with fly ash displays slower heating rate along with milder thermal gradient due to lower thermal conductivity of ash. Initial heating shows a lower gradient than MS-Sand. It has been noticed that the overall thermal transient is smoother due to dampening effect of ash. Thermal expansion up to ~0.25mm observed by 5 iterations. It has been also observed that, the value of temperature at steady state from Pocket 1 to 10 is 295 degrees and the temperature after 5th iteration lies in the range from 169 to 172 degrees approx.

Table 4.7 Transient Temperature Distribution in Rotor Blades (SS316 + Ash)

Blades No.	Temperature at Steady State (°C)	Temperature After 5th Iteration (°C)
Blade 1	295.4	212.8
Blade 2	295.4	212.9
Blade 3	295.5	208
Blade 4	295.6	204
Blade 5	295.7	199.7
Blade 6	295.3	195.1
Blade 7	295.3	194.9
Blade 8	295.2	200.8
Blade 9	295.1	205.2
Blade 10	295	209.2

4.11 Comparative Analysis: Convergence, Expansion and Clearance

Convergence Behavior:

- Mild Steel having higher thermal conductivity converges faster than SS 316.

- From the iteration count it became evident that among sand and ash the former shows quicker heat transfer than the latter one.

Temperature Distribution during Transient Period

- MS-Sand shows most uniform and fastest early heating.
- SS316-Ash shows slowest, steepest gradients, indicating thermal lag.

Expansion Effects:

- The SS316–Sand combination shows the greatest early thermal expansion (~0.48 mm), but stabilization occurs more slowly.
- Mild steel cases expand rapidly but also stabilize quickly due to higher thermal conductivity.

Impact on Clearance:

- The MS–Sand combination presents the highest risk of rapid clearance loss.
- The SS316–Ash combination has the lowest risk during the initial cycles; however, prolonged heat retention may impact long-term clearance and seal performance.

Conclusion

This study provides a detailed numerical analysis of the transient thermal behavior of rotary airlock valves (RALs) using different rotor materials (SS316 and mild steel) and powder types (sand and fly ash). The simulations revealed that mild steel reached steady state faster, requiring approximately 77–79 iterations and 231–237 seconds, compared to SS316 which required 95–97 iterations and 285–291 seconds. This faster convergence in mild steel is attributed to its higher thermal conductivity, which also contributed to lower maximum temperature differentials (0.4–0.5°C) compared to SS316 (0.7–0.8°C).

At steady state, the average pocket temperature stabilized around 295°C for all scenarios, but transient data showed that after 5 iterations, mild steel with sand had pocket temperatures between 172–175°C, whereas SS316 with sand reached higher intermediate temperatures of 197–216°C, indicating a slower but more retained heat buildup. Thermal expansion was highest for the SS316–sand combination (~0.48 mm) but stabilized more slowly, whereas mild steel cases expanded rapidly (~0.25–0.3 mm) and reached thermal equilibrium quicker. The material-powder combinations influenced clearance loss and sealing risks; mild steel with sand posed the highest risk due to rapid thermal expansion, while SS316 with ash showed the lowest initial risk but could face long-term clearance issues due to heat retention.

Overall, the findings demonstrate clear trade-offs: mild steel offers faster thermal response and quicker stabilization but less durability in harsh environments, while SS316 provides better corrosion resistance and fatigue life at the expense of longer warm-up times and localized overheating risk. The study validates numerical simulation as a robust tool for optimizing RAL design, guiding material selection, and improving operational safety in high-temperature powder handling.

Future Scope

While the present study has provided comprehensive simulation-based insights into the thermal behavior of rotary airlock valves, further work is necessary to enhance its practical applicability. Experimental validation of the simulated temperature distributions and thermal expansions is essential to confirm the accuracy of the numerical models. Controlled laboratory testing under representative operating conditions will provide critical data for this purpose. Additionally, exploring alternative rotor materials and surface coatings could offer improvements in thermal conductivity, reduce sintering effects, and enhance corrosion resistance, thereby extending valve life. Future studies should also focus on thermo-mechanical coupling to analyze the combined effects of thermal gradients and mechanical stresses on fatigue life and structural integrity. Optimization of seal design, specifically adaptive sealing technologies, is required to address clearance loss caused by thermal expansion and maintain operational efficiency. Finally, it is recommended that simulations be expanded to include dynamic factors such as rotor speed and cyclic thermal loading to better replicate real-world industrial conditions. These advancements will collectively contribute to the development of more reliable, efficient, and durable rotary airlock valves for high-temperature powder handling applications.

References:

[1] N. Somsuk, T. Wessapan, and S. Teekasap, “Design and Development of a Rotary Airlock Valve for Using in Continuous Pyrolysis Process to Improve Performance,” *Adv Mat Res*, vol. 383–390, pp. 7148–7154, Nov. 2011, doi: 10.4028/www.scientific.net/AMR.383-390.7148.

[2] C. R. Woodcock and J. S. Mason, “Components of pneumatic conveying systems,” in *Bulk Solids Handling*, Dordrecht: Springer Netherlands, 1987, pp. 408–437. doi: 10.1007/978-94-009-2635-6_13.

[3] N. Burdine, “Design of a pneumatic conveying test loop for laboratory testing.” [Online]. Available: https://scholar.utc.edu/honors-theses

[4] P. W. Wypych, “Effect of Rotary Valve Leakage on Pneumatic Conveying Performance,” *Particulate Science and Technology*, vol. 26, no. 3, pp. 257–272, Apr. 2008, doi: 10.1080/02726350802028975.

[5] T. L. Brown, P. Atluri, and J. P. Schmiedeler, “Design of High Speed Rotary Valves for Pneumatic Applications,” *Journal of Mechanical Design*, vol. 136, no. 1, Jan. 2014, doi: 10.1115/1.4025487.

[6] C. G. Toomey, “Pneumatic conveying system optimization,” *IEEE Trans Ind Appl*, vol. 50, no. 6, pp. 4319–4322, Nov. 2014, doi: 10.1109/TIA.2014.2346695.

[7] W. W. Meyer, “INDUSTRIAL SOLUTIONS.” [Online]. Available: www.meyerindustrial.com

[8] J. Rogers, M. S. A. Bradley, A. N. Pittman, R. J. Farnish, and A. R. Reed, “A simple analytical model for estimating air leakage through rotary valves,” *Proceedings of the Institution of Mechanical Engineers, Part E: Journal of Process Mechanical Engineering*, vol. 214, no. 3, pp. 185–196, Aug. 2000, doi: 10.1243/0954408001530047.

[9] P. W. Wypych and D. B. Hastie, “Theoretical Modelling of Rotary Valve Air Leakage for Pneumatic Conveying Theoretical Modelling of Rotary Valve Air Leakage for Pneumatic Conveying Systems Systems,” 2002. [Online]. Available: https://ro.uow.edu.au/engpapershttps://ro.uow.edu.au/engpapers/1287.https://ro.uow.edu.au/engpapers/1287

[10] M. Y. Gundogdu, “Design improvements on rotary valve particle feeders used for obtaining

suspended airflows," *Powder Technol*, vol. 139, no. 1, pp. 76–80, Jan. 2004, doi: 10.1016/j.powtec.2003.10.010.

[11] R. Siwek and C. Cesana, "Ignition Behavior of Dusts: Meaning and Interpretation."

[12] W. Wang, X. Si, H. Yang, H. Zhang, and J. Lu, "Heat-Transfer Model of the Rotary Ash Cooler Used in Circulating Fluidized-Bed Boilers," *Energy & Fuels*, vol. 24, no. 4, pp. 2570–2575, Apr. 2010, doi: 10.1021/ef100070n.

[13] R. Zhang, H. Yang, junfu Lu, and Y. Wu, "Theoretical and experimental analysis of bed-to-wall heat transfer in heat recovery processing," *Powder Technol*, vol. 249, pp. 186–195, Nov. 2013, doi: 10.1016/j.powtec.2013.08.017.

[14] S. Nagulmeera and M. Anilkumar, "Design, Modeling and Analysis of Rotary Air-Lock Valve."

[15] R. Siwek, "New knowledge about rotary air locks in preventing dust ignition breakthrough," *Plant/Operations Progress*, vol. 8, no. 3, pp. 165–176, Jul. 1989, doi: 10.1002/prsb.720080311.

[16] Jonathan O. Thorn, practical ways to handle rotary airlock valve leakage. 2007: Publicação Internacional Powder and Bulk Engineering, EUA

Altaf Warshi

RE-2022-637416

Universidad del Valle

Document Details

Submission ID
trn:oid:::26066:478459762

Submission Date
Aug 5, 2025, 10:57 AM GMT+5:30

Download Date
Aug 5, 2025, 10:59 AM GMT+5:30

File Name
RE-2022-637416.pdf

File Size
1.9 MB

59 Pages

14,393 Words

84,882 Characters

10% Overall Similarity

The combined total of all matches, including overlapping sources, for each database.

Filtered from the Report

- Bibliography
- Quoted Text

Match Groups

118 Not Cited or Quoted 9%
Matches with neither in-text citation nor quotation marks

21 Missing Quotations 1%
Matches that are still very similar to source material

0 Missing Citation 0%
Matches that have quotation marks, but no in-text citation

0 Cited and Quoted 0%
Matches with in-text citation present, but no quotation marks

Top Sources

5% Internet sources
5% Publications
7% Submitted works (Student Papers)

Integrity Flags

0 Integrity Flags for Review

No suspicious text manipulations found.

Our system's algorithms look deeply at a document for any inconsistencies that would set it apart from a normal submission. If we notice something strange, we flag it for you to review.

A Flag is not necessarily an indicator of a problem. However, we'd recommend you focus your attention there for further review.

Match Groups

- 118 Not Cited or Quoted 9%
  Matches with neither in-text citation nor quotation marks
- 21 Missing Quotations 1%
  Matches that are still very similar to source material
- 0 Missing Citation 0%
  Matches that have quotation marks, but no in-text citation
- 0 Cited and Quoted 0%
  Matches with in-text citation present, but no quotation marks

Top Sources

- 5% Internet sources
- 5% Publications
- 7% Submitted works (Student Papers)

Top Sources

The sources with the highest number of matches within the submission. Overlapping sources will not be displayed.

1	Internet	tudr.thapar.edu:8080 2%
2	Publication	Karan Sotoodeh. "The Comprehensive Valve Dictionary - Terminology, Application... <1%
3	Submitted works	Universiti Tenaga Nasional on 2025-06-03 <1%
4	Submitted works	International College of the Cayman Islands on 2025-07-28 <1%
5	Submitted works	Universiti Tenaga Nasional on 2016-02-19 <1%
6	Publication	R J Rogers. "A simple analytical model for estimating air leakage through rotary v... <1%
7	Submitted works	King Fahd University for Petroleum and Minerals on 2022-12-03 <1%
8	Publication	Wei Wang, Xiaodong Si, Hairui Yang, Hai Zhang, Junfu Lu. "Heat-Transfer Model o... <1%
9	Internet	link.springer.com <1%
10	Publication	Mehmet Yasar Gundogdu. "Design improvements on rotary valve particle feeders... <1%

11 Internet
c.coek.info <1%

12 Internet
edoc.pub <1%

13 Internet
www.readbag.com <1%

14 Publication
Ruiqing Zhang, Hairui Yang, junfu Lu, Yuxin Wu. "Theoretical and experimental a... <1%

15 Submitted works
University of Strathclyde on 2025-04-04 <1%

16 Submitted works
universititeknologimara on 2025-08-04 <1%

17 Submitted works
University of Wales, Lampeter on 2025-05-06 <1%

18 Internet
iaescore.com <1%

19 Internet
nova.newcastle.edu.au <1%

20 Internet
www.researchgate.net <1%

21 Publication
"Guidelines for Safe Handling of Powders and Bulk Solids", Wiley, 2004 <1%

22 Publication
"Experimental and Computational Fluid Mechanics", Springer Nature, 2014 <1%

23 Internet
www.coursehero.com <1%

24 Publication
Nisakorn Somsuk, Teerapot Wessapan, S. Teekasap. "Design and Development of ... <1%

25 Submitted works
University of Newcastle on 2023-07-17 <1%

26 Submitted works
University of Reading on 2025-04-08 <1%

27 Submitted works
Cranfield University on 2009-09-01 <1%

28 Publication
Park, Hee Sun, Young Jun Kim, Mi Hye Yu, Sung Il Jung, and Hae Jeong Jeon. "Shea... <1%

29 Publication
SFPE Handbook of Fire Protection Engineering, 2016. <1%

30 Publication
Ravi Inder Singh, Karan Ghule. "Design, development, experimental and CFD anal... <1%

31 Internet
umpir.ump.edu.my <1%

32 Publication
Grégory De Oliveira, Mireille Jacomino, Duy Long Ha, Stéphane Ploix. "Optimal po... <1%

33 Submitted works
Multimedia University on 2018-02-11 <1%

34 Internet
agris.fao.org <1%

35 Internet
www.pdfdrive.to <1%

36 Internet
www.sofa-framework.org <1%

37 Submitted works
Coventry University on 2024-05-10 <1%

38 Publication
Luana Boger Genaro, Thiago C. Souza Pinto, Alfredo M. Sarkis, Thiago Faggion de ... <1%

39 Internet
baixardoc.com <1%

40 Internet
www.meyerindustrial.com <1%

41 Publication
Alsoy-Akgün, Nagehan. "The Dual Reciprocity Boundary Element Solution of Helm... <1%

42 Publication
Chowdhry Amanullah, Mariyam Omran. "Using Machine Learning to Optimize Ad... <1%

43 Submitted works
Coventry University on 2013-05-08 <1%

44 Submitted works
Cranfield University on 2017-10-05 <1%

45 Submitted works
Malawi College of Accountancy on 2024-08-07 <1%

46 Submitted works
Universiti Tunku Abdul Rahman on 2017-08-25 <1%

47 Submitted works
University of Iowa on 2018-09-27 <1%

48 Submitted works
University of Ulster on 2007-03-27 <1%

49 Submitted works
University of Witwatersrand on 2020-02-20 <1%

50 Publication
C. R. Woodcock, J. S. Mason. "Bulk Solids Handling", Springer Nature, 1988 <1%

51 Publication
Jiawei, Zuo. "Numerical Investigation of Heat Transfer of a Multi-Layered Microch... <1%

52 Publication
Jin, Zetao. "Reduced-Order Modelling of Residual Stresses and Distortions in Weld... <1%

53 Submitted works
National Institute of Technology, Sri Nagar Jammu & Kashmir on 2020-07-03 <1%

54 Submitted works
Rose-Hulman Institute of Technology on 2025-06-19 <1%

55 Submitted works
The Robert Gordon University on 2022-08-17 <1%

56 Submitted works
The University of Manchester on 2019-09-02 <1%

57 Submitted works
Universiti Tenaga Nasional on 2015-02-17 <1%

58 Submitted works
University of Birmingham on 2017-03-13 <1%

59 Submitted works
University of Iowa on 2024-02-19 <1%

60 Submitted works
University of Sheffield on 2020-05-25 <1%

61 Submitted works
University of the West Indies on 2017-04-07 <1%

62 Internet
www.hbti.ac.in <1%

63 Internet
www.ros.hw.ac.uk <1%

64 Internet
www.tribology.rs <1%

65 Publication
Bolesław Karwat, Piotr Rubacha, Emil Stańczyk. "Numerical Simulations of the Ex... <1%

66 Publication
M. Samanta. "Efficient non-parametric estimation in the analysis of variance", Sta... <1%

67 Publication

P. W. Wypych. "Effect of Rotary Valve Leakage on Pneumatic Conveying Performa... <1%

68 Publication

Shengkai Tao, Qingbo Yu, Tianyu Kang, Zhongyuan Liu. "Experiment study and he... <1%

69 Submitted works

University of Glamorgan on 2020-03-28 <1%

70 Submitted works

University of Leeds on 2014-09-04 <1%

71 Publication

Nguyen Trung Thành, Hichem Sahli, Dinh Nho Hào. "Estimation of piecewise cons... <1%

72 Internet

stax.strath.ac.uk <1%

73 Internet

gecgudlavalleru.ac.in <1%

74 Internet

publications.lib.chalmers.se <1%